

Redox-Active Guanidine Ligands with Pyridine and *p*-Benzoquinone Backbones

Simone Stang,^[a] Anna Lebkücher,^[a] Petra Walter,^[a] Elisabeth Kaifer,^[a] and Hans-Jörg Himmel^{*[a]}

Keywords: Guanidine / Redox chemistry / Coordination compounds / Copper / Density functional calculations

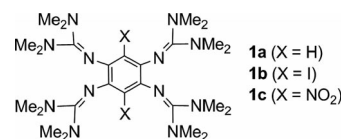
Herein we report on the synthesis and some aspects of the chemistry of the new redox-active ligands 2,3,5,6-tetrakis(tetramethylguanidino)pyridine, 2,3,5,6-tetrakis(tetramethylguanidino)-*p*-benzoquinone and 2,3,5,6-tetrakis(*N,N'*-dimethyl-*N,N'*-ethyleneguanidino)-*p*-benzoquinone. All three ligands are strong electron donors. In addition, the *p*-benzoquinone systems feature low LUMO energies and small

HOMO–LUMO gaps. A comparison of the ligands was made with regard to their optical properties, Brønsted basicity and electron-donor properties; results of quantum chemical calculations were included in this comparison. Subsequently, dinuclear copper complexes were prepared. Preliminary experiments on their redox chemistry followed.

Introduction

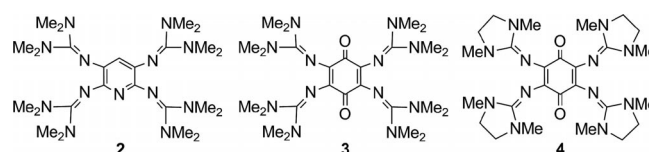
Aromatic compounds substituted with amino groups in pairs in the *para* or *ortho* positions have been known as electron donors for a long time. Examples include 1,4-dimethylamino-benzene,^[1] 1,2,4,5-tetrakis(dimethylamino)-benzene^[2] and 1,4,5,8-tetrakis(dimethylamino)naphthalene.^[3] The electron-donor strength can be further increased by the use of guanidino groups in place of the amino groups. Guanidines and guanidates have been shown to be versatile ligands,^[4–9] which have found applications in catalytic reactions such as lactide polymerization,^[10] and in the synthesis of complexes modeling enzymatic reactivity such as the biological dioxygen reduction cascade.^[11] The compound 1,2,4,5-tetrakis(tetramethylguanidino)benzene (**1a**) was the first member of a class of compounds named GFA-*n* (guanidino-functionalized aromatic compounds; *n* is the number of guanidino groups in pairs in the *para* positions).^[12] Because of the reduced steric demand of the guanidino groups in the vicinity of the basic imino N atoms, these compounds represent generally much better redox-active ligands than 1,2,4,5-tetrakis(dimethylamino)benzene. In the past, a number of dinuclear late-transition-metal complexes of **1a** was synthesized.^[13,14] The chemistry of copper complexes proved to be particularly interesting, and an almost complete charge-transfer series with examples for the complex types [Cu^I|**1a**|Cu^I], [Cu^I|**1a**²⁺|Cu^I] (in the form of a semiconducting coordination polymer), [Cu^{II}|**1a**|Cu^{II}],

[Cu^{II}|**1a**⁺|Cu^{II}] and [Cu^{II}|**1a**²⁺|Cu^{II}] were synthesized and completely characterized.^[13] Moreover, substitution of the two aromatic protons in **1a** by iodo or nitro groups (see Scheme 1) was shown to affect the HOMO and, in particular, the LUMO energy, which offers the opportunity of tuning the redox properties of the ligands.^[15]



Scheme 1. Structures of **1a** and of the products of further aromatic substitution, **1b** and **1c**.

In this work, we report on the synthesis and properties of the new redox-active guanidine ligands 2,3,5,6-tetrakis(tetramethylguanidino)pyridine (**2**), 2,3,5,6-tetrakis(tetramethylguanidino)-*p*-benzoquinone (**3**) and 2,3,5,6-tetrakis(*N,N'*-dimethyl-*N,N'*-ethyleneguanidino)-*p*-benzoquinone (**4**) shown in Scheme 2. These compounds are not just derivatives of **1a**; the additional function (pyridine N atom) introduced in compound **2** promises new possibilities. Especially, the addition of RX (e.g. R = alkyl, X = halide) to the [Cu^I|**2**|Cu^I] complexes might offer an access route to [Cu^I|(2-R)⁺|Cu^I] complexes (2-Me denotes the N_{pyridine}-



Scheme 2. Structures of the new electron donors studied in this work.

[a] Anorganisch-Chemisches Institut, Ruprecht-Karls-Universität Heidelberg, Im Neuenheimer Feld 270, 69120 Heidelberg, Germany
Fax: +49-6221-545707
E-mail: hans-jorg.himmel@aci.uni-heidelberg.de
Homepage: www.uni-heidelberg.de/institute/fak12/AC/himmel/index.htm

Supporting information for this article is available on the WWW under <http://dx.doi.org/10.1002/ejic.201200679>.

FULL PAPER

alkylated compound **2**). Moreover, oxidation of the cations (**2-R**)⁺ might lead to radical dications. Compounds **3** and **4** have distinct electronic properties; substituted *p*-benzoquinones are generally electron acceptors, and, therefore, **3** and **4** should exhibit LUMOs of low energies.

Results and Discussion

Ligand Synthesis and Properties

From the three new guanidine ligands described herein, the synthesis of **2** is the most straightforward. It was prepared in a two-step reaction according to Scheme 3. Reduction of 2,6-diamino-3,5-dinitropyridine (prepared by nitration of 2,6-diaminopyridine)^[16] with SnCl₂/HCl led to the protonated 2,3,5,6-tetraaminopyridine, which reacted with the “Vilsmeier salt” 2-chloro-1,1',3,3'-tetramethylformamidinium chloride in the presence of a base (NEt₃) to give the product in a 65% yield. Compound **2** can be crystallized from Et₂O solutions. Figure 1 shows its molecular structure. The aromatic carbon atom (from the C–H group) and the nitrogen atom of the pyridine ring could statistically change their positions in the crystal (with approximately equal probability for CH and N at both positions of the ring, see N7 and C3 in Figure 1).

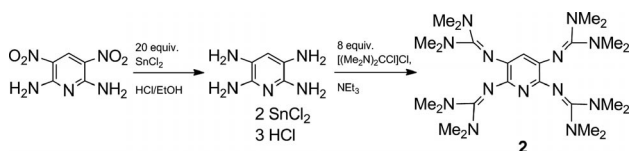
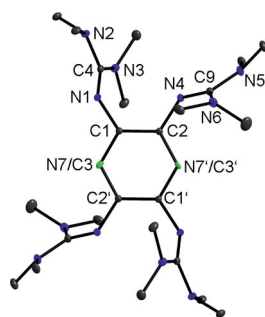
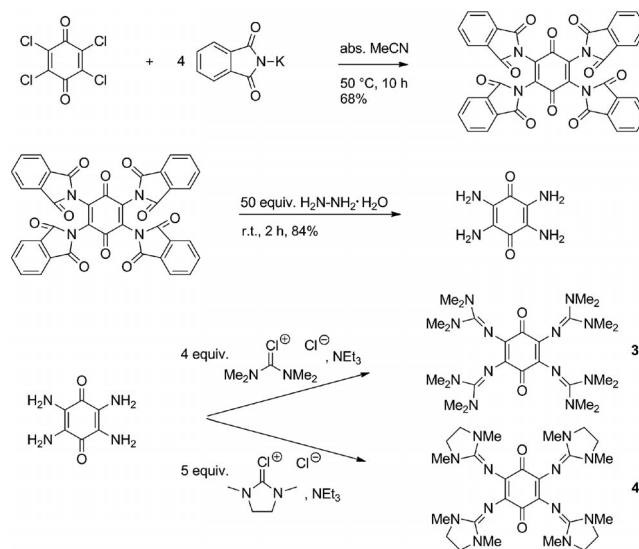
Scheme 3. Synthesis of **2**.

Figure 1. Molecular structure of **2**. Vibrational ellipsoids are drawn at the 50% probability level. Hydrogen atoms are omitted for the sake of clarity. Selected bond lengths (in pm) and bond angles (in degrees): N1–C1 140.43(11), N1–C4 128.86(12), N2–C4 140.18(12), N3–C4 137.72(13), N4–C2 140.99(11), N4–C9 129.95(12), N5–C9 137.32(11), N6–C9 139.08(13), N7–C1 136.77(12), N7–C2 137.11(12), C1–C2 141.25(12), C1–N1–C4 126.03(8), N2–C4–N3 113.17(8), C2–N4–C9 117.81(8), N5–C9–N6 114.07(8).

For the synthesis of **3**, the corresponding amine 2,3,5,6-tetrakis(amino)-*p*-benzoquinone (tabq) first had to be synthesized. This was accomplished in a two-step reaction

starting with 2,3,5,6-tetrachloro-*p*-benzoquinone (see Scheme 4).^[17,18] Reaction with 2-chloro-1,1',3,3'-tetramethylformamidinium chloride, [(Me₂N)₂CCl]Cl, then yielded 2,3,5,6-tetrakis(tetramethylguanidino)-*p*-benzoquinone (**3**). In addition, the product of elimination of two dimethylamino groups followed by cyclization was crystallized in a small amount {2,6-bis(dimethylamino)benzo[1,2-*d*:4,5-*d'*]-diimidazole-4,8(1*H*,5*H*)dione, see Supporting Information}. A similar side-product was already isolated in the synthesis of **1a**.^[15] Deep green crystals of **3** were obtained from CH₃CN. Its structure is shown in Figure 2. The C₆ ring and the two O atoms occupy one plane, in contrast to the situation found in tetrakis(dimethylamino)-*p*-benzoquinone.^[19] Hence, it could be concluded that the steric situation is relaxed. As anticipated, the C1–C2 bond [136.11(19) pm in **3**] is considerably shorter than the C1–C3' or C2–C3 bonds [148.90(19) and 148.66(18) pm, respectively]. The variations in the C–C bond lengths are comparable with those for related benzoquinones such as 2,3,5,6-tetrakis(dimethylamino)-*p*-benzoquinone (with C–C bond lengths of 137, 146 and 151 pm).^[19] The C=O bond length of 123.42(2) pm in **3** also is close to that reported for 2,3,5,6-tetrakis(dimethylamino)-*p*-benzoquinone.^[19] By using a similar protocol as for the synthesis of **3**, compound **4** was synthesized. Crystals of this compound could be grown from CH₃CN solutions. Its molecular structure is also included in Figure 2. Again, the C₆ ring and the O atoms are in the same plane, which shows that the steric demand of the guanidino groups is significantly smaller than that of the amino groups in 2,3,5,6-tetrakis(dimethylamino)-*p*-benzoquinone.^[19]

Scheme 4. Synthesis of **3** and **4**.

The optical spectra of the guanidine electron donors have been shown to change dramatically upon oxidation and are valuable indicators for the oxidation state. The UV/Vis spectra of **2** (see Supporting Information) contain two intense bands, centred at $\lambda_{\text{max}} = 208$ and 253 nm in CH₃CN

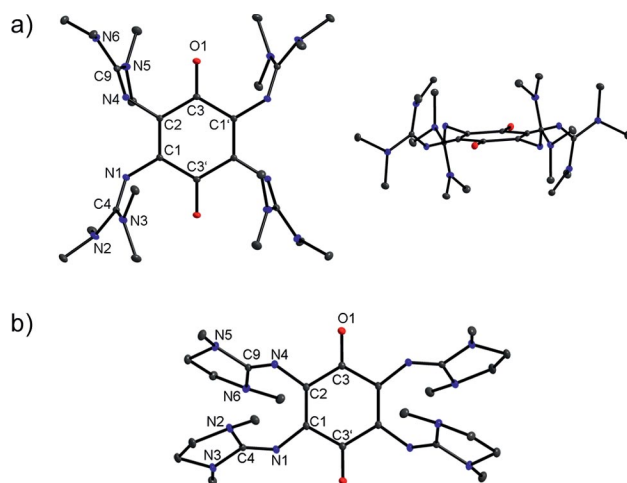


Figure 2. Molecular structure of (a) **3** and (b) **4**. Hydrogen atoms are omitted for the sake of clarity. Thermal ellipsoids are drawn at the 50% probability level. Selected bond lengths (in pm) and bond angles (in degrees) for **3**: O1–C3 123.42(16), N1–C1 138.98(17), N1–C4 130.27(17), N2–C4 137.31(18), N3–C4 137.45(18), N4–C2 139.12(17), N4–C9 129.72(18), N5–C9 138.27(19), N6–C9 137.18(17), C1–C2 136.11(19), C1–C3' 148.90(19), C2–C3 148.66(18), C1–N1–C4 122.49(12), C2–N4–C9 121.19(12), N2–C4–N3 115.34(12), N5–C9–N6 115.51(12). Selected bond lengths (in pm) and bond angles (in degrees) for **4**: O1–C3 122.64(15), N1–C1 138.35(15), N1–C4 129.26(16), N2–C4 138.32(17), N3–C4 137.50(15), N4–C2 138.31(15), N4–C9 128.57(15), N5–C9 138.79(15), N6–C9 137.66(16), C1–C2 136.63(17), C1–C3' 149.32(16), C2–C3 149.12(17), C1–N1–C4 125.92(11), N2–C4–N3 108.13(10), C2–N4–C9 126.35(11), N5–C9–N6 108.11(10).

and 208 and 243 nm in Et₂O, which can be assigned to transitions localized at the pyridine ring. For comparison, three absorption bands were reported for pyridine at $\lambda_{\max} = 172$, 194 and 248 nm.^[20] The two bands at $\lambda_{\max} = 331$ and 360 nm in CH₃CN and 323 and 358 nm in Et₂O solution can be assigned to transitions involving orbitals to which the guanidino groups contribute. A corresponding band at 329 nm is observed in the case of **1a** dissolved in CH₃CN solution.^[12] CH₃CN solutions of **3** are slightly fluorescent. The emission spectrum presented in Figure 3 shows signals at 286 and 560 nm. The absorption that corresponds to the 560 nm emission is virtually not visible in the UV/Vis spectrum. On the other hand, the 286 nm emission signal corresponds to the 215 nm absorption, which translates into a relatively large Stokes shift of 71 nm. Fluorescence in *p*-benzoquinone derivatives is rare, but not unprecedented. König observed fluorescence for the molecule 2-(β -hydroxyethylamino)-*p*-benzoquinone, while other quinones such as 2-amino- and 2,5-diamino-*p*-benzoquinones are fluorescence-silent.^[21] For this molecule, a quinone–quinol equilibrium was found in solution (see Scheme 5).^[22] Therefore, we synthesized this species again and compared its fluorescence with that of **3**. We were, to the best of our knowledge for the first time, able to crystallize the molecule in its quinol form from MeOH solution. A visualization of the structure alongside with a list of selected structural parameters

is included in the Supporting Information. The absorption spectrum is governed by two strong absorptions at $\lambda_{\max} = 226$ and 360 nm. The emission spectrum features signals at 345 nm for excitation at 226 nm and 485 nm for excitation at 360 nm. Hence, the spectra are significantly different to those of **3**. Quantum chemical calculations on **3** found no energy minimum for a possible isomer with the quinol structure. The push–pull type situation has to be taken into account to explain the distinct optical properties of **3**, and an equilibrium between two isomers can be ruled out.

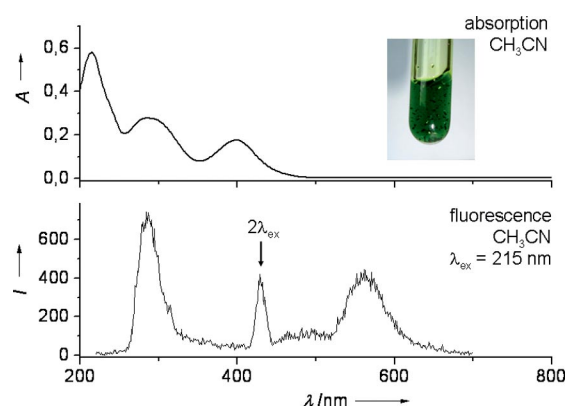
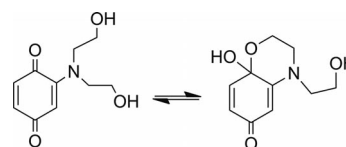


Figure 3. Absorption and emission spectra recorded for CH₃CN solutions of **3**.



Scheme 5. Example for an experimentally observed quinone–quinol equilibrium.

In Figure 4, the colours of CH₃CN solutions of four different redox-active guanidine ligands are compared. While compound **1a** is colourless, derivative **2** is slightly yellow and **3** has an intense green colour. The intense red colour of **1c** can also be seen.^[15]

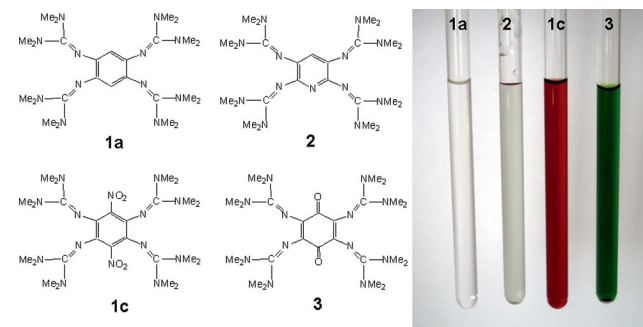


Figure 4. Photo showing the different colours of CH₃CN solutions of the four organic electron donors **1a**, **2**, **1c** and **3**.

In Figure 5 the energies of the HOMOs and LUMOs calculated by DFT methods (B3LYP/6-311G**) are compared for the three ligands **1a**, **2** and **3**. Moreover, the electron-

FULL PAPER

density distribution in these two orbitals is visualized for **2** and **3**. The HOMO in all cases is centred at the C₆ ring. In the case of **3**, the orbitals of the LUMO have considerable character from the C=O group (π^* orbital), which leads to a significant reduction of the LUMO energy. The HOMO–LUMO gap shrinks from 4.4 and 4.3 eV for **1a** and **2**, respectively, to only 2.4 eV for **3**. For comparison, in compound **1c**, the gap is calculated to be 2.9 eV.^[15] The experimental and quantum chemical results show that the optical properties could be varied over a large region, making these ligands especially attractive for the synthesis of redox-active complexes.

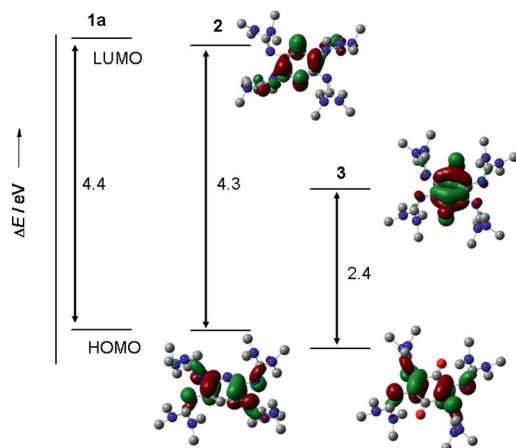


Figure 5. Comparison between the HOMO–LUMO energy gap calculated (B3LYP/6-311G**) for the guanidine ligands **1a**, **2** and **3**. Although the absolute LUMO energies cannot reliably be calculated by DFT methods, the energy differences can be treated with more confidence.

In addition to the basic guanidino groups, the new compounds **2–4** exhibit basic sites with the pyridine N atom in **2** and the oxygen atoms of the *p*-benzoquinone systems **3** and **4**. Reaction of **2** with excess HCl resulted in tetraprotonation. The salt $[2H_4]Cl_4 \cdot 2H_2O$ could be crystallized from hot CH₃CN solutions (see the structure derived from XRD in Figure 6a). Reaction of **3** with HCl afforded the salt $[3H_4]Cl_4 \cdot 10H_2O$ (see Figure 6b). In crystalline **3**, a network was established by hydrogen bonding involving the guanidine N–H, co-crystallized water molecules and the chloride counterions.

While all four imino N atoms of the guanidino groups were protonated, the pyridine N atom in **2** or the O atoms in **3** were not attacked. Protonation is in both cases accompanied by an increase in the N=C bond length and a decrease in the C–NMe₂ single bond lengths. 2,3,5,6-Tetrakis(amino)-*p*-benzoquinones were shown to undergo distinct colour changes upon HCl addition.^[23] For example, 2,3,5,6-tetrakis(dimethylamino)-*p*-benzoquinone, which gives black–brown DMF solutions, adopts first a deep blue and then a yellow–red colour upon HCl addition. In the case of **3**, the colour changes from deep green to red. Quantum chemical calculations (B3LYP/6-311G*) were carried out to compare $2H^+$ and $3H^+$, in which protonation occurs at the imino N atom; tautomers arise from protonation at

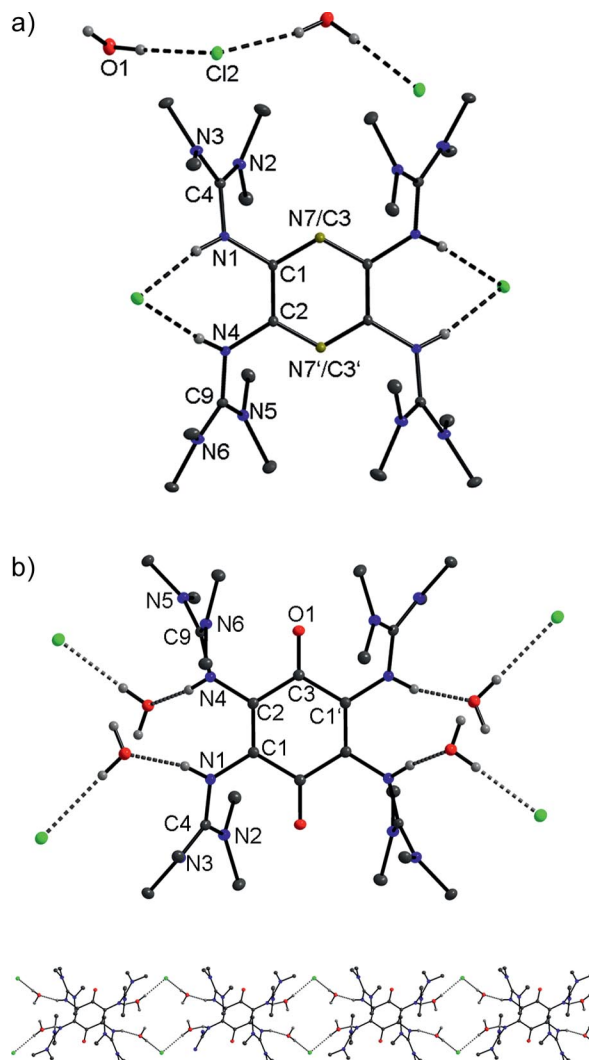
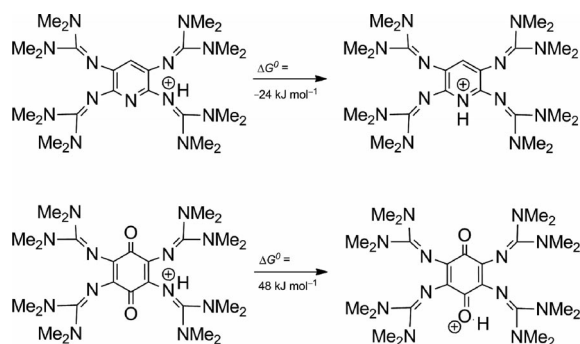


Figure 6. (a) Fraction of the crystal structure of $[2H_4]Cl_4 \cdot 2H_2O$. Vibrational ellipsoids are drawn at the 50% probability level. Selected bond lengths (in pm) and bond angles (in degrees): N1–C1 141.22(18), N1–C4 135.89(18), N2–C4 133.10(18), N3–C4 133.89(18), N4–C2 140.99(17), N4–C9 136.52(18), N5–C9 133.40(18), N6–C9 132.64(18), C1–C2 139.30(19), C1–N7/C3 135.64(18), C2–N7'/C3' 135.81(18), C1–N1–C4 122.21(11), N2–C4–N3 121.23(13), C2–N4–C9 121.76(11), N5–C9–N6 121.36(13). (b) Molecular structure of $[3H_4]Cl_4 \cdot 10H_2O$. Hydrogen atoms are omitted for the sake of clarity. Thermal ellipsoids are drawn at the 50% probability level. Selected bond lengths (in pm) and bond angles (in degrees): O1–C3 122.1(2), N1–C1 139.5(2), N1–C4 137.2(2), N2–C4 132.6(2), N3–C4 132.7(2), N4–C2 140.0(2), N4–C9 136.4(2), N5–C9 133.2(2), N6–C9 133.1(2), C1–C2 135.1(2), C2–C3 148.1(2), C3–C1' 149.3(2), C1–N1–C4 125.29(15), N2–C4–N3 122.16(16), C2–N4–C9 125.04(14), N5–C9–N6 121.66(15). The network established through hydrogen bonding can be visualized below.

the pyridine nitrogen atom (in the case of **2**) or the *p*-benzoquinone C=O group (in the case of **3**). According to these calculations, gas-phase protonation at the pyridine N atom in **2** is slightly favoured over protonation at the guanidino groups ($\Delta G^0 = -24 \text{ kJ mol}^{-1}$). In contrast, for **3**, protonation at the carbonyl group is clearly disfavoured ($\Delta G^0 = +48 \text{ kJ mol}^{-1}$) (see Scheme 6).



Scheme 6. Comparison between protonation at the guanidino groups and the pyridine N atom in **2** or the O atom in **3**.

Moreover, an empirical formula provided by Maksić et al.^[24] was employed to estimate the $pK(\text{BH}^+)$ value of 2H^+ (protonation at the guanidino group) in CH_3CN on the basis of quantum chemical calculations. A $pK(\text{BH}^+)$ value of 24.6 was obtained. In a similar way, the $pK(\text{BH}^+)$ value for 3H^+ in CH_3CN was estimated to be 23.9. For comparison, a $pK(\text{BH}^+)$ value of 25.3 in CH_3CN was derived for **1a**.^[25] Thus, the compounds could be ordered with regard to their Brønsted basicity as $3 < 2 < 1\text{a}$.

Redox Chemistry

The electron donor capacity was then studied by cyclic voltammetry (CV) (see Figure 7) and redox reactions. The CV results are summarized in Table 1. The CV curve of **2** (Bu_4NPF_6 as electrolyte, scan speed 100 mV s^{-1}) shows a sharp reversible two-electron wave at $E_{1/2}(\text{CH}_2\text{Cl}_2) = -0.30 \text{ V vs. Ag/AgCl}$ or $-0.76 \text{ V vs. Fc/Fc}^+$ ($\text{Fc} = \text{ferrocene}$, see Figure 7a). Virtually the same value was obtained for **1a**.^[12] Quantum chemical calculations (B3LYP/6-311G**) gave a ΔG^0 value of not more than $+1.5 \text{ kJ mol}^{-1}$ for the gas-phase electron transfer reaction between **1a** and 2^{2+} outlined in Scheme 7. Hence, the quantum chemical calculations are in line with the experimental results and predict the donor capacity of **1a** and **2** to be similar. In agreement with this finding, the HOMO energies were calculated to be similar (see Figure 5). A reversible one-electron wave, corresponding to the oxidation to the trication, occurs at $E_{1/2}(\text{CH}_2\text{Cl}_2) = 1.32 \text{ V vs. Ag/AgCl}$ or $0.86 \text{ V vs. Fc/Fc}^+$. This value is clearly higher than that measured for **1a** (0.68 V , also vs. Fc/Fc^+) (see Table 1). Figure 7b displays the CV curve for **3** dissolved in CH_2Cl_2 (vs. Ag/AgCl), measured at a scan rate of 100 mV s^{-1} with Bu_4NPF_6 as electrolyte. A reduction wave was not observed. It presumably lies below -1.5 V . For comparison, the $E_{1/2}(\text{DMF})$ vs. SCE value decreases from -0.40 V in *p*-benzoquinone to -1.07 V in 2,3,5,6-tetrakis(dimethylamino)-*p*-benzoquinone.^[19] The LUMO energy of **3**, although significantly lower than that for **1a**, is still too high for reduction to be observed within the measured potential window. A relatively sharp reversible two-electron oxidation wave appears at $E_{1/2}(\text{CH}_2\text{Cl}_2) = -0.16 \text{ V vs. Ag/AgCl}$ or $-0.62 \text{ V vs. Fc/Fc}^+$. Two further reversible one-electron oxidation waves were observed at

$E_{1/2}(\text{CH}_2\text{Cl}_2) = 0.91$ and $1.21 \text{ V vs. Ag/AgCl}$, which corresponds to $E_{1/2}(\text{CH}_2\text{Cl}_2) = 0.45$ and $0.74 \text{ V vs. Fc/Fc}^+$. The introduction of four highly basic guanidino functions turns the *p*-benzoquinone system from an electron acceptor into a relatively strong electron donor. Quantum chemical calculations on the thermodynamics of the gas-phase electron transfer reaction between neutral **1a** and the dication 3^{2+} to give 1a^{2+} and **3** gave a ΔG^0 value of $-19.3 \text{ kJ mol}^{-1}$ (see

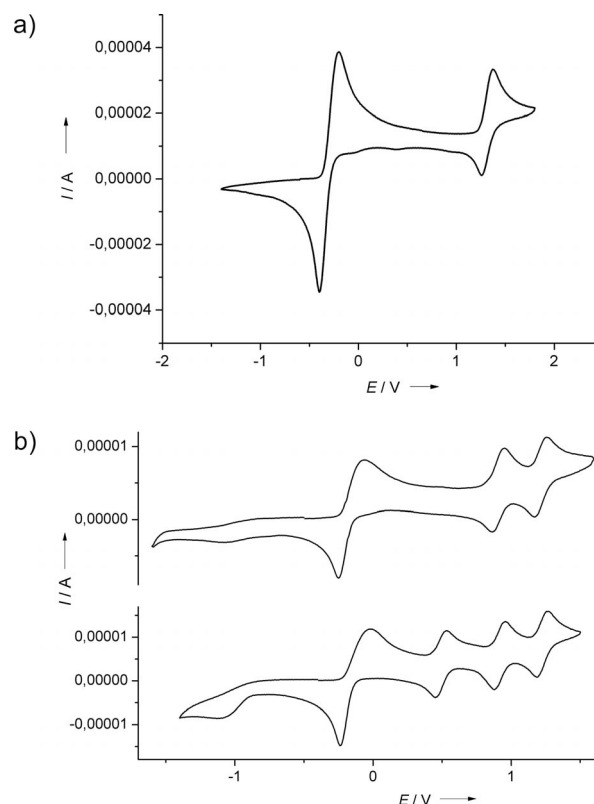
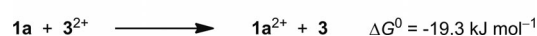


Figure 7. CV curves (CH_2Cl_2 , supporting electrolyte Bu_4NPF_6 , reference electrode Ag/AgCl , scan rate 100 mV s^{-1}) for (a) **2** (without addition of ferrocene) and (b) **3** (without and with ferrocene added as internal standard).

Table 1. Observed E values (in V, vs. $\text{Cp}_2\text{Fe/Cp}_2\text{Fe}^+$) from CV (CH_2Cl_2 solution).

	1st wave (two-electron)			2nd wave (one-electron)			3rd wave (one-electron)		
	E_{ox}	E_{red}	$E_{1/2}$	E_{ox}	E_{red}	$E_{1/2}$	E_{ox}	E_{red}	$E_{1/2}$
1a	-0.71	-0.82	-0.76	0.72	0.65	0.68	–	–	–
2	-0.65	-0.85	-0.76	0.92	0.80	0.86	–	–	–
3	-0.51	-0.73	-0.62	0.47	0.39	0.43	0.78	0.70	0.74

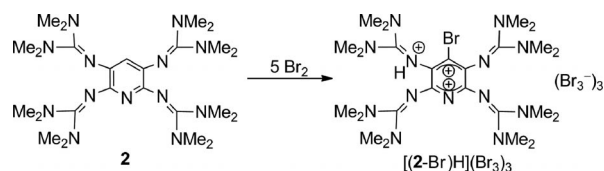


Scheme 7.

FULL PAPER

Scheme 7). Hence the calculations are again in line with the CV results, which indicate that **3** is a slightly weaker electron donor than **1a**. Consequently, the HOMO energy is lower by 0.28 eV for **3** than for **1a** (see Figure 5).

The guanidine groups could also be oxidized by chemical means. We were especially interested in obtaining information about the structure and optical properties of the oxidized free ligands, which can then be compared with the data observed after oxidation of the dinuclear (copper) complexes. In the case of the reaction between **2** and Br₂, oxidation was accompanied by aromatic substitution (see Scheme 8). The proton released in this process bonds to one of the imino N atoms. The salt $[(2\text{-Br})\text{H}](\text{Br}_3)_3$ crystallizes upon addition of toluene to the CH₃CN solution. Figure 8a shows its structure, and selected structural parameters can be found in the figure caption. On the basis of these parameters, the dication can be best described as a pair of bis-guanidino-allyl cations connected by two C–C single bonds [C1–C2 and C4–C5, with bond lengths of 149.2(4) and 151.4(4) pm, respectively]. In a similar way, reaction with I₂ resulted in oxidation and substitution. In this case, the salts $(2\text{-I})(\text{I}_3)\text{I}$ and $(2\text{-I})_2$ were isolated from the reaction mixture (see Figure 9 and Supporting Information). Protonation was not observed in this case.



Scheme 8. Oxidation of **2** with Br₂.

Besides the structural information, the absorption spectra are characteristic of the oxidized ligands. The spectra of the free ligands could serve as reference for the analysis of the electronic properties in oxidized dinuclear complexes. The two-electron oxidation of **2** was accompanied by a colour change of the solution from pale yellow to deep red. Figure 9 shows as an example the UV/Vis spectrum of solutions of $(2\text{-I})(\text{I}_3)\text{I}$. The absorption maxima were detected at 245, 290, 366 and 513 nm. The broad 366 nm band appears to be composed of two features; a shoulder is marginally visible at 390 nm. The band at 290 nm together with one of the features of the 366 nm band can be assigned to the I₃[−] anion [cf. 292 and 363 nm reported if the anion was formed by reaction between I₂ and $(n\text{-C}_4\text{H}_9)_4\text{NI}$ in CH₃CN^[26]].

Oxidation of **3** with I₂ in a CH₂Cl₂ solution furnished the salt $(3)\text{I}_2$. Crystals were obtained directly from the solution (see Figures 10 and 11a). Most remarkably, the C=C bond length of 136.11(2) pm (C1–C2) in neutral **3** increases by more than 9 ppm [to 145.7(4) pm] upon two-electron oxidation. At the same time, the N=C bond lengths of 130.27(2) (N1–C4) and 129.72(2) pm (N4–C9) in neutral **3** increase to 136.5(4) and 136.7(4) pm, respectively. In contrast, the bond lengths between the N atom of the guanidino group and the C atom of the central C₆ ring (N1–

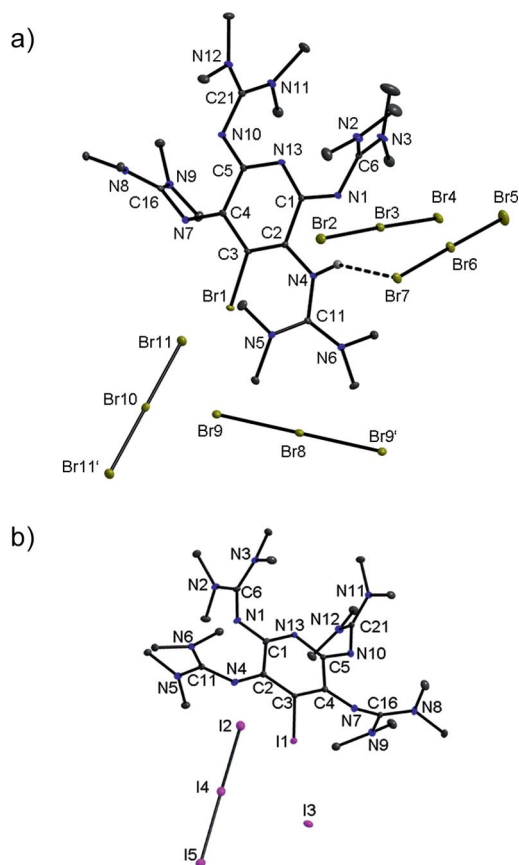
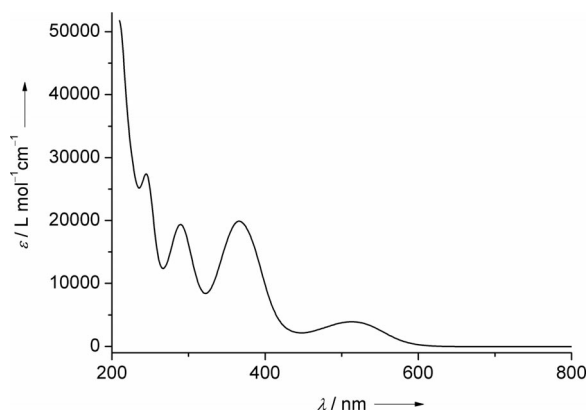
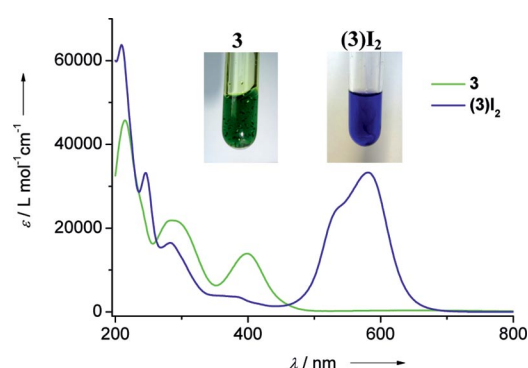


Figure 8. Fractions of the crystal structures of (a) $[(2\text{-Br})\text{H}](\text{Br}_3)_3$ and (b) $(2\text{-I})(\text{I}_3)\text{I}$. Vibrational ellipsoids are drawn at the 50% probability level. Selected bond lengths (in pm) and bond angles (in degrees) for $[(2\text{-Br})\text{H}](\text{Br}_3)_3$: Br1–C3 188.3(3), N1–C1 129.9(3), N1–C6 137.0(4), N2–C6 132.8(4), N3–C6 132.8(4), N4–C2 137.7(3), N4–C11 138.9(4), N5–C11 132.0(4), N6–C11 131.6(4), N7–C4 128.0(4), N7–C16 138.5(4), N8–C16 132.2(4), N9–C16 134.0(4), N10–C5 130.1(4), N10–C21 138.7(4), N11–C21 133.2(4), N12–C21 132.5(4), N13–C1 133.9(3), N13–C5 134.6(3), C1–C2 149.2(4), C2–C3 134.9(4), C3–C4 145.4(4), C4–C5 151.4(4), C1–N1–C6 121.1(2), N2–C6–N3 122.4(3), C2–N4–C11 131.9(2), N5–C11–N6 123.2(3), C4–N7–C16 126.4(2), N8–C16–N9 122.3(3), C5–N10–C21 117.3(2), N11–C21–N12 123.4(3). Selected bond lengths (in pm) and bond angles (in degrees) for $(2\text{-I})(\text{I}_3)\text{I}$: I2–I4 290.75(8), I4–I5 298.19(9), I1–C3 209.4(4), N1–C1 132.5(6), N1–C6 136.3(6), N2–C6 133.2(6), N3–C6 135.1(6), N4–C11 136.1(6), N5–C11 133.7(7), N6–C11 132.9(6), N7–C4 131.0(6), N7–C16 134.1(6), N8–C16 132.7(6), N9–C16 135.5(7), N10–C5 129.7(6), N10–C21 137.5(6), N11–C21 133.4(6), N12–C21 134.1(6), N13–C1 133.7(6), N13–C5 135.0(6), C1–C2 151.8(6), C2–C3 141.0(6), C3–C4 137.2(6), C4–C5 153.1(6), I2–I4–I5 172.896(18), C1–N1–C6 120.0(4), C2–N4–C11 129.0(4), C4–N7–C16 128.2(4), C5–N10–C21 119.2(4), N2–C6–N3 120.6(4), N5–C11–N6 120.7(4), N8–C16–N9 118.8(4), N11–C21–N12 120.7(4).

C1 and N4–C2, see Figure 11) decrease by more than 8 pm [138.98(2) and 139.12(2) pm before and 130.6(4) and 130.5(4) pm after oxidation]. In the same way, the salt $(4)\text{I}_2$ could be prepared by reaction of **4** with I₂ (see Figure 11b). Solutions of $(3)\text{I}_2$ and $(4)\text{I}_2$ are deep blue or purple. The UV/Vis spectra of neutral and dicationic **3** are compared in Figure 10. The spectrum of $(3)\text{I}_2$ shows a strong and broad absorption at 581 nm.

Figure 9. UV/Vis spectrum of [2-I](I₃)I dissolved in Et₂O.Figure 10. Comparison between the UV/Vis spectra of neutral **3** and (**3**)₂.

Coordination Compounds

Reaction between **2** and 2 equiv. CuBr or CuI furnished the dinuclear complexes [2(CuBr)₂] and [2(CuI)₂] (Scheme 9). Their structures are presented in Figure 12. All bonding parameters indicate a strong ligand–metal bonding. The imino C=N bonds of the guanidino groups [131.9(4) and 132.7(4) pm] are elongated with respect to those of free **2** [128.86(12) and 129.95(12) pm], which indicates the presence of ligand–metal π bonding in addition to σ bonding.^[27] Because of the strong Lewis basicity of **2**, the copper metal is “satisfied” with a relatively low coordination number of 3. The geometry of the complexes is only slightly distorted – the two halide–Cu–N angles and Cu–N bond lengths are slightly different.

In addition, we reacted **2** with 2 equiv. CuCN. Again, complex formation proved possible, and yellow crystals of the dinuclear complex [2(CuCN)₂] were grown from CH₃CN solutions. Figure 13 displays its molecular structure, which is similar to those of [2(CuBr)₂] and [2(CuI)₂].

These three complexes of the type [Cu^I]₂[Cu^I] could serve as starting points for oxidation experiments aiming at the synthesis of an electron transfer series. First, we reacted [2(CuI)₂] with I₂. The product is the coordination polymer {[2-I](CuI)₂}(I₃)₂]_n, which represents an example for the type [Cu^I]₂[2⁺][Cu^I]. As observed in the experiment with the free ligand, oxidation is accompanied by aromatic substitu-

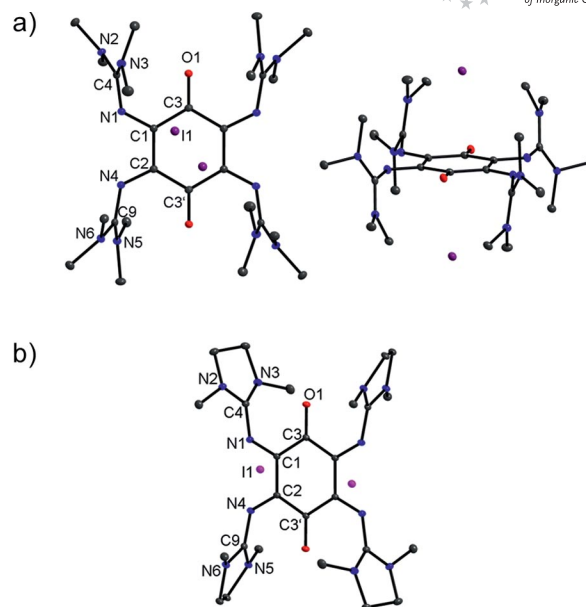


Figure 11. Fraction of the crystal structures of (a) (**3**)₂ and (b) (**4**)₂. Vibrational ellipsoids are drawn at the 50% probability level. Hydrogen atoms are omitted for the sake of clarity. Selected bond lengths (in pm) and bond angles (in degrees) for (**3**)₂: O1–C3 124.4(3), N1–C1 130.6(4), N1–C4 136.5(4), N2–C4 133.2(4), N3–C4 134.5(4), N4–C2 130.5(4), N4–C9 136.7(4), N5–C9 133.0(4), N6–C9 134.2(4), C1–C2 145.7(4), C1–C3' 146.0(4), C2–C3 146.8(4), C1–N1–C4 124.9(3), N2–C4–N3 120.5(3), C2–N4–C9 125.3(3), N5–C9–N6 121.2(3). Selected bond lengths (in pm) and bond angles (in degrees) for (**4**)₂: O1–C3 124.0(2), N1–C1 130.5(2), N1–C4 135.6(2), N2–C4 133.4(3), N3–C4 134.2(2), N4–C2 130.1(2), N4–C9 136.1(2), N5–C9 132.9(2), N6–C9 133.7(2), C1–C2 145.6(2), C1–C3 146.8(2), C1–N1–C4 125.44(16), N2–C4–N3 111.39(16), C2–N4–C9 127.02(16), N5–C9–N6 111.68(16).

Scheme 9. Reaction of **2** with Cu^I compounds.

tion. Crystals of this compound were grown from acetonitrile solutions. Unfortunately, the quality was not high enough for a detailed structural analysis. Nevertheless, preliminary analysis indicate that the compound consists of 1D cationic chains, in which the Cu atoms are tetra-coordinated and connected together by two iodo bridges. The complex [2(CuI)₂] did not react with CH₃I both at room temperature and at 48 °C (Scheme 10).

Reaction between **3** and CuI resulted in a product mixture, from which a small amount of black crystalline material was isolated; structural analysis confirms a 1D coordination polymer [3(CuI)(CuI₂)I]_n (see Figure 14), in which the copper atoms are connected by one iodo bridge. The structural data indicate that guanidine **3** is twofold oxidized and coordinated by Cu^I. Hence, this compound represents the first coordination compound of the general type [Cu^I]₂[3²⁺][Cu^I].

FULL PAPER

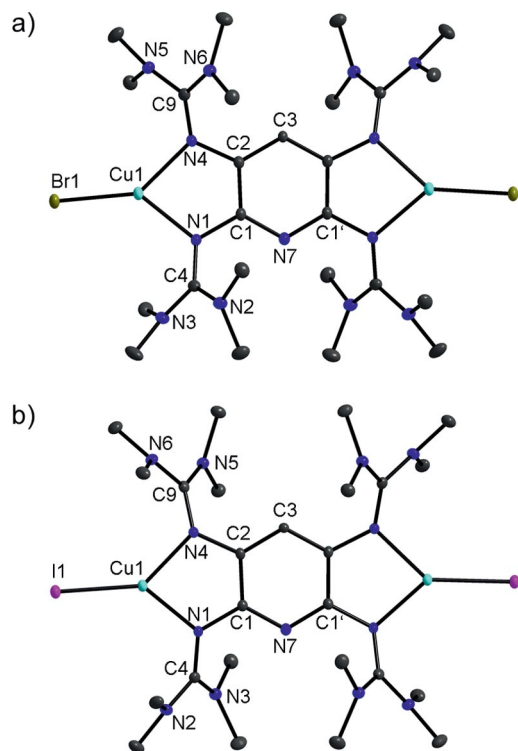


Figure 12. Molecular structures of (a) $[2(\text{CuBr})_2]$ and (b) $[2(\text{CuI})_2]$. Vibrational ellipsoids are drawn at the 50% probability level. Hydrogen atoms are omitted for the sake of clarity. Selected bond lengths (in pm) and bond angles (in degrees) for $[2(\text{CuBr})_2]$: Cu1–Br1 228.76(9), Cu1–N1 201.8(2), Cu1–N4 203.1(2), N1–C1 139.6(3), N1–C4 132.7(4), N2–C4 135.3(4), N3–C4 135.5(4), N4–C2 140.7(4), N4–C9 131.9(4), N5–C9 136.1(4), N6–C9 135.8(4), N7–C1 135.4(3), C1–C2 140.3(4), C2–C3 138.2(3), N1–Cu1–N4 83.12(10), N1–Cu1–Br1 136.13(7), N4–Cu1–Br1 140.73(7). Selected bond lengths (in pm) and bond angles (in degrees) for $[2(\text{CuI})_2]$: Cu1–I1 244.58(10), Cu1–N1 201.0(2), Cu1–N4 203.3(2), N1–C1 140.1(3), N1–C4 133.0(3), N2–C4 135.4(4), N3–C4 135.6(4), N4–C2 141.7(3), N4–C9 131.4(3), N5–C9 137.0(4), N6–C9 137.0(4), N7–C1 134.3(3), C1–C2 141.0(4), C2–C3 137.7(3), N1–Cu1–N4 83.69(9), N1–Cu1–I1 137.94(6), N4–Cu1–I1 138.36(6).

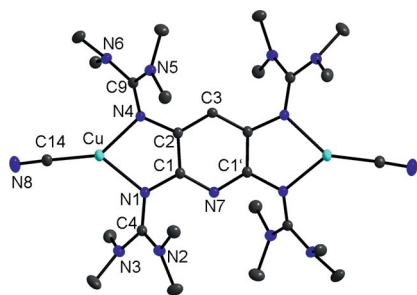
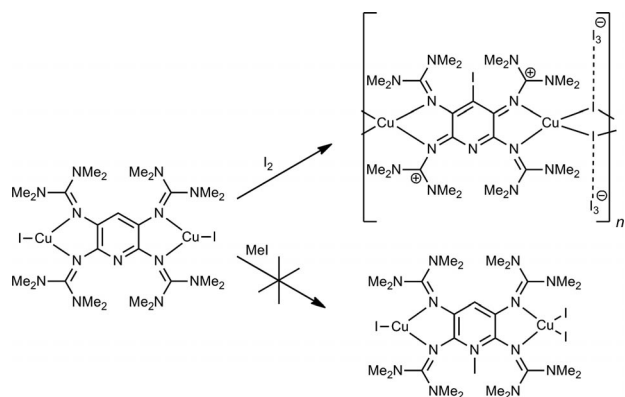


Figure 13. Molecular structure of $[2(\text{CuCN})_2]$. Vibrational ellipsoids are drawn at the 50% probability level. Hydrogen atoms are omitted for the sake of clarity. Selected bond lengths (in pm) and bond angles (in degrees): Cu–N1 202.88(19), Cu–N4 202.74(19), Cu–C14 186.1(3), N1–C1 140.4(3), N1–C4 132.9(3), N2–C4 135.7(3), N3–C4 135.7(3), N4–C9 132.2(3), N5–C9 136.8(3), N6–C9 136.1(3), N7–C1 134.3(3), N8–C14 115.5(3), C1–C2 141.0(3), C2–C3 138.3(3), N1–Cu–N4 82.34(8), N1–Cu–C14 134.69(10), N4–Cu–C14 142.96(10).



Scheme 10. Experiments to probe the reactivity of $[2(\text{CuI})_2]$.

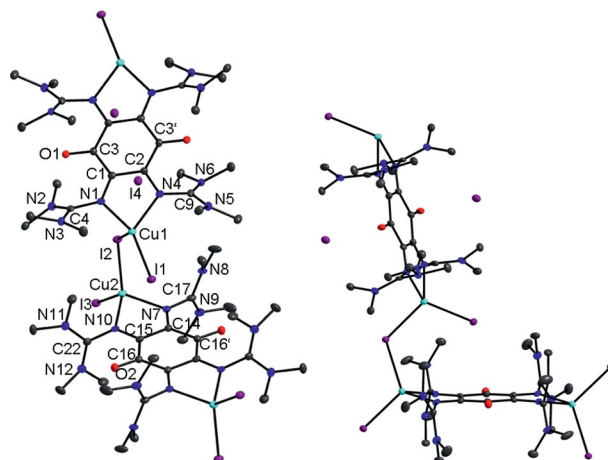


Figure 14. Part of the structure of the polymer $[\text{Cu}(\text{I})_2]_n$, from two perspectives. Hydrogen atoms are omitted for the sake of clarity. Selected bond lengths (in pm) and bond angles (in degrees): Cu1–I1 255.06(13), Cu1–I2 260.25(13), Cu1–N1 209.1(6), Cu1–N4 211.4(6), Cu2–I2 258.64(15), Cu2–I3 254.76(12), Cu2–N7 211.3(6), Cu2–N10 208.7(6), N1–C1 129.5(9), N1–C4 138.8(9), N2–C4 133.1(9), N3–C4 133.9(9), N4–C2 133.4(9), N4–C9 138.3(9), N5–C9 131.1(9), N6–C9 132.1(10), C1–C2 145.8(10), C1–C3 145.3(9), N1–Cu1–N4 78.2(2), I1–Cu1–I2 113.50(5), I2–Cu2–I3 116.01(4), N7–Cu2–N10 77.0(2).

Conclusions

In this work, we reported the synthesis of the new redox-active ligands 2,3,5,6-tetrakis(tetramethylguanidino)pyridine (**2**), 2,3,5,6-tetrakis(tetramethylguanidino)-*p*-benzoquinone (**3**) and 2,3,5,6-tetrakis(*N,N'*-dimethyl-*N,N'*-ethylene-guanidino)-*p*-benzoquinone (**4**). Compounds **3** and **4** feature high HOMO and low LUMO energies, which result in small HOMO–LUMO gaps and intensely green solutions. The properties and reactivity were discussed on the basis of experimental results as well as quantum chemical (DFT) calculations. The discussion especially concentrated on the optical properties, Brønsted basicity and electron donor capacity. A comparison between the ligands before and after oxidation is of importance to understand the electronic properties of their complexes. Dinuclear copper complexes were then synthesized. In preliminary experiments on the redox chemistry of these complexes, we oxidized the

complex $[2(\text{CuI})_2]$ with I_2 to give the coordination polymer $\{[(2\text{-I})(\text{CuI})_2](\text{I}_3)_2\}_n$ with dicationic ligand units. Reaction of **3** with CuI leads directly to a 1D coordination polymer $[3(\text{CuI})(\text{CuI}_2)\text{I}]_n$ with oxidized ligand units.

Experimental Section

All synthetic work was carried out under an inert gas atmosphere by using standard Schlenk techniques. All solvents were rigorously dried prior to their use. NMR spectra were measured on a DRX-200, Bruker Avance II 400 or a Bruker Avance III 600 spectrometer. A Cary 5000 spectrophotometer was used for UV/Vis spectroscopy. For IR spectroscopy, CsI discs of the compounds were measured with a FTIR Biorad Merlin Excalibur FT 3000 spectrometer. Elemental analyses were carried out at the Microanalytical Laboratory of the University of Heidelberg. An EG&G Princeton 273 apparatus was used for the CV measurements. The curves were recorded at different scan rates in the range 50–200 mV s⁻¹ with an Ag/AgCl electrode as reference electrode and Bu₄NPF₆ (Fluka, electrochemical grade) as electrolyte. HR-EI spectra were recorded on a JEOL JMS-700 magnetic sector, ESI and HR-ESI spectra on a Finnigan LCQ quadrupole ion trap and FAB spectra were recorded on a MAT 8230. 2,6-Diamino-3,5-dinitropyridine^[16] and 2,3,5,6-tetraaminobenzoquinone^[17,18] were synthesized according to reported procedures. All other reagents were of reagent-grade quality as obtained from commercial suppliers and were used without further purification.

2,3,5,6-Tetraaminopyridine (tap): A suspension of 2,6-diamino-3,5-dinitro-pyridine (2.00 g, 10.05 mmol) in EtOH (75 mL) was added to a solution of SnCl₂ (38.11 g, 200.9 mmol) in concentrated HCl (100 mL). The suspension was stirred for 2.5 h at a temperature of 40 °C. The reaction mixture was then allowed to cool to room temperature. A pale yellow solid precipitated. The solution was removed by filtration, and the solid washed several times with EtOH to yield tap·2SnCl₂·3HCl (4.65 g, 7.43 mmol, 74%). ¹H NMR (199.92 MHz, DMSO): δ = 7.80–8.80 (br. s, 8 H, NH₂), 7.43 (s, 1 H, H_{Ar}) ppm. MS(EI⁺): *m/z* (%) = 139.1 (97.08) [tap]⁺, 124.2 (100.0) [tap-NH₂]⁺. C₅H₁₂N₅·2SnCl₂·3HCl (627.77): calcd. C 9.57, H 1.93, N 11.16; found C 9.66, H 2.07, N 10.82.

2,3,5,6-Tetrakis(tetramethylguanidino)pyridine (2): *N,N,N',N'*-Tetramethylurea (3.8 mL, 3.68 g, 31.66 mmol) was dissolved in CHCl₃ (25 mL). After dropwise addition of oxalyl chloride (13.90 mL, 20.22 g, 159.3 mmol), the reaction mixture was stirred for 16 h under reflux. The solution was then cooled back to room temperature, and the solvent removed under vacuum. The remaining solid was washed three times with 15 mL portions of Et₂O and dried under vacuum. Subsequently, the colourless solid was redissolved in CH₃CN (30 mL). This solution was added slowly to a suspension of tap·2SnCl₂·3HCl (2.199 g, 3.51 mmol) in CH₃CN (40 mL) and NEt₃ (10 mL) kept at a temperature of 0 °C. An orange suspension was formed which was stirred for 4 h at 0 °C. The orange solution was removed by a cannula, and the remaining orange solid washed three times with 10 mL portions of CH₃CN. It was then dissolved in a 10% HCl solution (10 mL). Subsequently, a 25% NaOH solution (20 mL) was added, and the reaction mixture extracted with Et₂O (5 × 100 mL). The combined organic phases were dried with K₂CO₃, and the solvent removed with a rotary evaporator to yield **2** (1.21 g, 2.27 mmol, 65%) as a pale green solid. Recrystallization from Et₂O afforded crystals suitable for XRD analysis. C₂₅H₄₉N₁₃ (531.74): calcd. C 56.47, H 9.29, N 34.24; found C 56.18, H 9.17, N 33.94. ¹H NMR (399.89 MHz, CD₃CN): δ = 5.86 (s, 1 H, H_{Ar}), 2.64 (s, 24 H, CH₃), 2.62 (s, 24 H, CH₃)

ppm. ¹³C{¹H} NMR (100.56 MHz, CD₃CN), HSQC, HMBC: δ = 160.16 (s, NCN), 158.94 (s, NCN), 148.55 (s, C_{Ar}), 133.45 (s, C_{Ar}), 123.17 (d, C_{Ar}, CH), 39.96 (q, CH₃) ppm. MS (HR-EI⁺): *m/z* (%) = 531.4240 (100) [M]⁺(calcd. 531.4233). IR (CsI): $\tilde{\nu}$ = 2997 (w), 2931 (w), 2885 (w), 2804 (w), 1608 (vs), 1562 (vs), 1508 (s), 1458 (s), 1419 (s), 1377 (s), 1141 (s), 1018 (m), 894 (w), 725 (w), 671 (w) cm⁻¹. UV/Vis (CH₃CN): λ (ε, L mol⁻¹ cm⁻¹) = 360 (11050), 331 (11047), 253 (19906), 208 (41062) nm. UV/Vis (Et₂O): λ (ε, L mol⁻¹ cm⁻¹) = 358 (17142), 323 (13295), 243 (36855), 208 (53270) nm. Crystal data for C₂₅H₄₉N₁₃: *M*_r = 531.77, 0.40 × 0.40 × 0.35 mm, monoclinic, space group *P*2₁/*n*, *a* = 9.892(2), *b* = 11.025(2), *c* = 13.816(3) Å, β = 97.39(3), *V* = 1494.3(5) Å³, *Z* = 2, *d*_{calcd.} = 1.182 Mg m⁻³, Mo-*K*_α radiation (graphite monochromated, λ = 0.71073 Å), *T* = 100 K, θ_{range} 2.37 to 33.16°. Reflections measured 11249, independent 5662, *R*_{int} = 0.0317. Final *R* indices [*I* > 2σ(*I*): *R*₁ = 0.0466, *wR*₂ = 0.1153.

2,3,5,6-Tetrakis(tetramethylguanidino)-*p*-benzoquinone (3): Oxalyl chloride (2.075 mL, 3.019 g, 23.79 mmol) was added dropwise to a solution of tetramethyl urea (0.571 mL, 0.553 g, 4.758 mmol) in CHCl₃ (15 mL). Subsequently, the reaction mixture was stirred for 16 h under reflux. The solvent was then removed under vacuum. The remaining solid was washed three times with 10 mL portions of Et₂O, dried and dissolved in CH₃CN (12 mL). This solution was slowly added at a temperature of 0 °C to a suspension of 2,3,5,6-tetraaminobenzoquinone (0.200 g, 1.199 mmol) in 12 mL of CH₃CN and NEt₃ (1.989 mL, 1.444 g, 14.27 mmol). The suspension was gradually warmed from 0 °C to room temperature (over a period of 4.5 h). Subsequently, the solvent was removed under vacuum, which left a green–grey solid residue. This residue was dissolved in an HCl solution (10 mL of a 10% solution), which led to a dark red solution. After addition of a NaOH solution (10 mL of a 25% solution), the solution turned dark green. The solution was then extracted several times with Et₂O, until the Et₂O phase remained colourless. The combined organic phases were dried with K₂CO₃, and the solvent then removed under vacuum. Yield: 90.30 mg (0.16 mmol, 14%) in the form of a green solid recrystallized from CH₃CN. C₂₆H₄₈N₁₂O₂ (560.76): calcd. C 55.69, H 8.63, N 29.97; found C 55.44, H 8.63, N 28.32. ¹H NMR (600.13 MHz, CD₃CN): δ = 2.69 (s, CH₃) ppm. ¹³C{¹H} NMR (150.90 MHz, CD₃CN), HSQC, HMBC: δ = 183.26 (s, C=O), 161.87 (s, NCN), 135.69 (s, C_{ring}), 39.40 (q, CH₃) ppm. MS (HR-EI⁺): *m/z* (%) = 560.4022 (100) [M]⁺ (calcd. 560.4023). IR (CsI): $\tilde{\nu}$ = 2997 (w), 2932 (m), 2882 (m), 2801 (w), 1597 (s), 1562 (vs), 1508 (s), 1458 (m), 1423 (m), 1381 (s), 1346 (m), 1285 (m), 1223 (s), 1142 (s), 1107 (w), 1049 (m), 988 (s), 976 (s), 914 (m), 806 (w), 760 (m), 733 (w), 710 (w), 671 (w), 640 (w), 563 (w), 552 (w), 525 (w) cm⁻¹. UV/Vis (CH₃CN): λ (ε, L mol⁻¹ cm⁻¹) = 398 (13919), 286 (21840), 215 (45746) nm. Crystal data for C₂₆H₄₈N₁₂O₂: *M*_r = 560.76, 0.35 × 0.32 × 0.25 mm, monoclinic, space group *C*2/*c*, *a* = 24.037(5) Å, *b* = 12.855(3) Å, *c* = 10.874(2) Å, β = 113.58(3)°, *V* = 3079.5(13) Å³, *Z* = 4, *d*_{calcd.} = 1.209 Mg m⁻³, Mo-*K*_α radiation (graphite monochromated, λ = 0.71073 Å), *T* = 100 K, θ_{range} 1.83 to 32.05°. Reflections measured 10283, independent 5331, *R*_{int} = 0.0514. Final *R* indices [*I* > 2σ(*I*): *R*₁ = 0.0557, *wR*₂ = 0.1353.

2,3,5,6-Tetrakis(*N,N'*-dimethyl-*N,N'*-ethylene-guanidino)-*p*-benzoquinone (4): Oxalyl chloride (1.297 mL, 1.887 g, 14.87 mmol) was dropwise added to a solution of 1,3-dimethylimidazolidine-2-one (0.321 mL, 0.339 g, 2.974 mmol) in CHCl₃ (12 mL). Subsequently, the solution was stirred under reflux for 16 h. The solvent was then removed under vacuum, and the remaining solid residue washed three times with 10 mL portions of Et₂O. The solid residue was then dried and redissolved in CH₃CN (6 mL). The solution was slowly added at 0 °C to a suspension of 2,3,5,6-tetrakis(amino)-

FULL PAPER

benzoquinone (0.100 g, 0.5947 mmol) in CH₃CN (6 mL). The reaction mixture was gradually warmed up from 0 °C to room temperature over a period of 5 h. The solvent was then removed under vacuum, and the remaining residue dissolved in H₂O (5 mL). A NaOH solution (7 mL of a 25% solution) was added to this green-brown solution, which led to a deep green solution. The solution was then extracted with CH₃CN, until the organic phase remained colourless. The combined organic phases were dried with K₂CO₃, and the solvent removed under vacuum to yield the crude product (300.7 mg, 0.54 mmol, 91%) in the form of a green solid. Recrystallization from a CH₃CN/C₇H₈ mixture gave crystals of **4** suitable for an XRD analysis. C₂₆H₄₀N₁₂O₂ (552.70): calcd. C 56.50, H 7.29, N 30.41; found C 54.95, H 7.37, N 29.56. ¹H NMR (600.13 MHz, CD₃CN): δ = 3.20 [dd (m), *J* = 16.94, *J* = 4.23 Hz, 16 H, CH₂], 2.65 (s, 24 H, CH₃) ppm. ¹³C{¹H} NMR (150.90 MHz, CD₃CN), HSQC, HMBC: δ = 183.70 (s, C=O), 155.67 (s, NCN), 134.68 (s, C_{ring}), 48.79 (t, CH₂), 34.23 (q, CH₃) ppm. ¹H NMR (600.13 MHz, CD₂Cl₂): δ = 3.23 (m, 16 H, CH₂), 2.70 (s, 24 H, CH₃) ppm. ¹³C{¹H} NMR (150.90 MHz, CD₂Cl₂), HSQC, HMBC: δ = 183.38 (s, C=O), 155.62 (s, NCN), 134.21 (s, C_{ring}), 48.72 (t, CH₂), 34.33 (q, CH₃) ppm. MS (HR-EI⁺): *m/z* (%) = 552.3420 (100) [M]⁺ (calcd. 552.3397), (9.02) [M]²⁺ (calcd. 276.1761). IR (CsI): $\tilde{\nu}$ = 2940 (w), 2862 (w), 2831 (w), 1655 (s), 1597 (m), 1493 (w), 1458 (w), 1443 (w), 1412 (w), 1393 (w), 1335 (w), 1315 (m), 1288 (m), 1238 (m), 1192 (w), 1169 (w), 1138 (w), 1122 (w), 1080 (w), 1030 (m), 999 (m), 984 (w), 968 (m), 949 (s), 860 (w), 802 (w), 768 (w), 748 (w), 706 (w), 671 (w), 652 (w), 633 (w), 610 (w), 579 (w), 532 (w), 505 (w) cm⁻¹. UV/Vis (CH₃CN): λ (ε, L mol⁻¹ cm⁻¹) = 400 (14237), 277 (28614) nm. Crystal data for C₂₆H₄₀N₁₂O₂: *M_r* = 552.70, 0.50 × 0.40 × 0.40 mm, monoclinic, space group *P*2₁/*c*, *a* = 9.839(2) Å, *b* = 13.628(3) Å, *c* = 10.650(2) Å, β = 93.31(3)°, *V* = 1425.6(5) Å³, *Z* = 2, *d*_{calcd.} = 1.288 Mg m⁻³, Mo-*K*_α radiation (graphite monochromated, λ = 0.71073 Å), *T* = 100 K, θ_{range} 2.43 to 30.03°. Reflections measured 8134, independent 4163, *R*_{int} = 0.0315. Final *R* indices [*I* > 2σ(*I*): *R*₁ = 0.0464, *wR*₂ = 0.1183.

2-(β-Hydroxy-ethylamino)-*p*-benzoquinone: The compound was synthesized as described in the literature (yield: 70%)^[26] and crystallized from MeOH solutions. Crystal data for C₁₀H₁₃NO₄: *M_r* = 422.43, 0.50 × 0.50 × 0.40 mm, monoclinic, space group *P*2₁/*n*, *a* = 8.4980(17) Å, *b* = 12.451(3) Å, *c* = 8.9990(18) Å, β = 93.14(3)°, *V* = 950.7(3) Å³, *Z* = 2, *d*_{calcd.} = 1.476 Mg m⁻³, Mo-*K*_α radiation (graphite monochromated, λ = 0.71073 Å), *T* = 100 K, θ_{range} 2.91 to 27.91°. Reflections measured 2546, independent 1789, *R*_{int} = 0.0377. Final *R* indices [*I* > 2σ(*I*): *R*₁ = 0.0486, *wR*₂ = 0.1211.

[2H₄]Cl₄: Compound **2** (60.0 mg, 0.11 mmol) was dissolved in Et₂O (10 mL). To this pale green solution, HCl in EtOH (0.4 mL of a 1 M solution) was added. A pale yellow solid precipitated from the cloudy solution. The solution was stirred for 30 min at room temperature, and the solvent was then removed under vacuum. The remaining colourless residue was crystallized from hot CH₃CN (3 mL) to yield colourless crystals of [2H₄]Cl₄·2H₂O (58.9 mg, 0.083 mmol, 73%). ¹H NMR (399.89 MHz, CD₃CN): δ = 11.72 (s, 2 H, NH), 11.33 (s, 2 H, NH), 7.43 (s, 1 H, H_{Ar}), 3.03 (s, 24 H, CH₃), 3.00 (s, 24 H, CH₃) ppm. ¹³C{¹H} NMR (100.56 MHz, CD₃CN), HSQC, HMBC: δ = 159.37 (s, NCN), 158.90 (s, NCN), 141.42 (s, C_{Ar}), 129.09 (s, C_{Ar} CH), 123.34 (d, C_{Ar}), 41.71 (q, CH₃) ppm. MS (ESI⁺): *m/z* (%) = 532.3 (60.11) [2H]⁺, 266.7 (100.0) [2H₂]⁺. Crystal data for [2H₄]Cl₄·2H₂O, C₂₅H₅₇Cl₄N₁₃O₂: *M_r* = 713.64, 0.20 × 0.20 × 0.15 mm, monoclinic, space group *P*2₁/*n*, *a* = 8.2090(16), *b* = 25.283(5), *c* = 9.769(2) Å, β = 111.29(3)°, *V* = 1889.2(8) Å³, *Z* = 2, *d*_{calcd.} = 1.255 Mg m⁻³, Mo-*K*_α radiation (graphite monochromated, λ = 0.71073 Å), *T* = 100 K, θ_{range} 2.38

to 29.99°. Reflections measured 10807, independent 5509, *R*_{int} = 0.0269. Final *R* indices [*I* > 2σ(*I*): *R*₁ = 0.0410, *wR*₂ = 0.1007.

[3H₄]Cl₄: Compound **3** (10.0 mg, 0.018 mmol) was dissolved in CH₃CN (2 mL). A solution of HCl in Et₂O (0.4 mL of a 0.2 M solution, 0.08 mmol) was then added, and the colour of the solution changed from green to red. The reaction mixture was stirred at room temperature for 1 h. Subsequently, the solution was concentrated and stored at 0 °C to afford dark red crystals. ¹H NMR (200 MHz, CD₃CN): δ = 10.61 (s, 4 H, NH), 3.04 (s, 48 H, CH₃) ppm. Crystal data for C₂₆H₇₂Cl₄N₁₂O₁₂: *M_r* = 886.76, 0.20 × 0.16 × 0.16 mm, monoclinic, space group *P*2₁/*n*, *a* = 11.128(2) Å, *b* = 15.468(3) Å, *c* = 13.767(3) Å, β = 108.30(3)°, *V* = 2249.8(9) Å³, *Z* = 2, *d*_{calcd.} = 1.309 Mg m⁻³, Mo-*K*_α radiation (graphite monochromated, λ = 0.71073 Å), *T* = 100 K, θ_{range} 2.04 to 27.48°. Reflections measured 10259, independent 5145, *R*_{int} = 0.0370. Final *R* indices [*I* > 2σ(*I*): *R*₁ = 0.0437, *wR*₂ = 0.1124.

[(2-Br)H](Br)₃: Compound **2** (30.0 mg, 0.056 mmol) was dissolved in CH₃CN (6 mL). Then Br₂ (8.69 μL, 27.0 mg, 0.17 mmol) was then added to the pale green solution. Brown crystals precipitated from the brown reaction mixture after addition of toluene (6 mL). Yield: 38.1 mg, 0.028 mmol (51% relative to **2**, 83% relative to bromine). C₂₅H₄₉Br₁₀N₁₃ (1330.78): calcd. C 22.56, H 3.71, N 13.68; found C 23.02, H 3.89, N 14.10. ¹H NMR (399.89 MHz, CD₃CN): δ = 8.39 (s, 1 H, NH), 3.13 (s, 12 H, CH₃), 3.02 (s, 24 H, CH₃), 2.98 (s, 12 H, CH₃) ppm. ¹³C{¹H} NMR (100.56 MHz, CD₃CN), HSQC, HMBC: δ = 41.87 (q, CH₃) ppm. MS (ESI⁺): *m/z* (%) = 687.9 (80.11) [2-Br]²⁺Br⁻, 304.8 (100.0) [2-Br]²⁺. UV/Vis (Et₂O): λ (ε, L mol⁻¹ cm⁻¹) = 360 (11870), 269 (82736) nm. Crystal data for C₂₅H₄₉Br₁₀N₁₃: *M_r* = 1330.77, 0.35 × 0.35 × 0.30 mm, monoclinic, space group *P*2₁/*c*, *a* = 21.190(4) Å, *b* = 13.057(3) Å, *c* = 17.766(4) Å, β = 112.67(3)°, *V* = 4536(2) Å³, *Z* = 4, *d*_{calcd.} = 1.949 Mg m⁻³, Mo-*K*_α radiation (graphite monochromated, λ = 0.71073 Å), *T* = 100 K, θ_{range} 2.08 to 33.14°. Reflections measured 32211, independent 17183, *R*_{int} = 0.0455. Final *R* indices [*I* > 2σ(*I*): *R*₁ = 0.0423, *wR*₂ = 0.0823.

[2-I](I₃): Compound **2** (30.3 mg, 0.057 mmol) was dissolved in CH₃CN (5 mL), and I₂ (28.9 mg, 0.11 mmol) added to the pale green solution. The reaction mixture turned deep red. Red crystals were obtained after addition of toluene (5 mL). C₂₅H₄₈I₅N₁₃·0.5 toluene (1211.32): calcd. C 28.26, H 4.34, N 15.03; found C 28.50, H 4.34, N 15.06. ¹H NMR (399.89 MHz, CD₃CN): δ = 2.92 (s, 24 H, CH₃), 2.91 (s, 24 H, CH₃) ppm. ¹³C{¹H} NMR (100.56 MHz, CD₃CN), HSQC, HMBC: δ = 169.91 (s, NCN), 167.54 (s, NCN), 155.85 (s), 154.52 (s), 83.26 (s, CI), 41.60 (q, CH₃), 41.13 (q, CH₃) ppm. MS (ESI⁺): *m/z* (%) = 657.5 (16.11) [2-I]⁺, 531.3 (10.51) [2]⁺, 328.7 (23.01) [2-I]²⁺, 265.8 (100) [2]²⁺. UV/Vis (Et₂O): λ (ε, L mol⁻¹ cm⁻¹) = 513 (7870), 366 (39795), 290 (38726), 245 (54800) nm. Crystal data for C₃₂H₅₆I₅N₁₃: *M_r* = 1257.40, 0.30 × 0.15 × 0.15 mm, monoclinic, space group *Cc*, *a* = 15.983(3), *b* = 15.896(3), *c* = 17.995(4) Å, β = 97.28(3)°, *V* = 4535.1(16) Å³, *Z* = 4, *d*_{calcd.} = 1.842 Mg m⁻³, Mo-*K*_α radiation (graphite monochromated, λ = 0.71073 Å), *T* = 100 K, θ_{range} 2.28 to 32.09°. Reflections measured 48382, independent 15614, *R*_{int} = 0.0457. Final *R* indices [*I* > 2σ(*I*): *R*₁ = 0.0389, *wR*₂ = 0.0956.

[2-I]₂: Compound **2** (30.3 mg, 0.057 mmol) was dissolved in CH₂Cl₂ (5 mL), and I₂ (28.9 mg, 0.11 mmol) added to the pale green solution. The reaction mixture turned deep red. Red crystals were obtained after addition of Et₂O (5 mL). ¹H NMR (600.13 MHz, CD₃CN): δ = 2.93 (s, 24 H, CH₃), 2.91 (s, 24 H, CH₃) ppm. ¹³C{¹H} NMR (150.90 MHz, CD₃CN), HSQC, HMBC: δ = 169.88 (s, NCN), 167.52 (s, NCN), 155.83 (s), 154.49 (s), 83.31 (s, CI), 41.64 (q, CH₃), 41.15 (q, CH₃) ppm. Crystal data for [2-I]

Redox-Active Guanidine Ligands with Pyridine and *p*-Benzoquinone Backbones

$\text{I}_2 \cdot \text{CH}_2\text{Cl}_2$, $\text{C}_{26}\text{H}_{50}\text{Cl}_3\text{I}_2\text{N}_{13}$: $M_r = 996.39$, $0.30 \times 0.25 \times 0.25$ mm, tetragonal, space group $P4(3)$, $a = 11.4730(16)$, $b = 11.4730(16)$, $c = 33.024(7)$ Å, $V = 4346.9(12)$ Å³, $Z = 4$, $d_{\text{calcd.}} = 1.522$ Mg m⁻³, Mo- K_{α} radiation (graphite monochromated, $\lambda = 0.71073$ Å), $T = 100$ K, $\theta_{\text{range}} 2.47$ to 27.45° . Reflections measured 9845, independent 9840, $R_{\text{int}} = 0.0417$. Final R indices [$I > 2\sigma(I)$]: $R_1 = 0.0606$, $wR_2 = 0.1704$.

(3)I₂: Compound **3** (16.8 mg, 0.030 mmol) was dissolved in CH_2Cl_2 (5 mL), and I_2 (7.60 mg, 0.030 mmol) was added. The colour of the solution turned from dark green to dark blue. Black crystals with a red metallic shine were obtained by layering the solution with Et_2O (5 mL). $\text{C}_{26}\text{H}_{48}\text{I}_2\text{N}_{12}\text{O}_2 \cdot 3\text{CH}_2\text{Cl}_2$ (1069.35): calcd. C 32.57, H 5.09, N 15.72; found C 32.32, H 5.07, N 16.36. ¹H NMR (600.13 MHz, CD_3CN): $\delta = 2.91$ (s, CH_3) ppm. ¹³C{¹H} NMR (150.90 MHz, CD_3CN), HSQC, HMBC: $\delta = 171.68$ (s, NCN), 168.10 (s, C=O), 149.81 (s, C_{ring}), 41.12 (q, CH_3) ppm. MS (HR-ESI⁺): m/z (%) = 687.30641 (39.4) $[\text{M} - \text{I}]^+$ (calcd. 687.30680), 560.40185 (82.7) $[\text{M} - \text{I}_2]^+$ (calcd. 560.40177), 280.20063 (100.0) $[\text{M} - \text{I}_2]^{2+}$ (calcd. 280.20061). IR (CsI): $\tilde{\nu} = 2997$ (w), 2957 (m), 2917 (m), 2797 (w), 1599 (s), 1559 (m), 1504 (vs), 1448 (m), 1397 (vs), 1357 (m), 1292 (m), 1320 (w), 1171 (m), 1062 (s), 1000 (w), 898 (m), 797 (w), 768 (m), 727 (m), 688 (w), 656 (m), 608 (w), 569 (w), 549 (w), 494 (w), 473 (w), 458 (w), 419 (m) cm⁻¹. UV/Vis (CH_3CN): λ (ϵ , L mol⁻¹ cm⁻¹) = 581 (33284), ca. 535 (24720), ca. 378 (3657), 282 (16476), 246 (33171), 209 (63756) nm. Crystal data for **(3)I₂·2CH₂Cl₂**, $\text{C}_{28}\text{H}_{52}\text{Cl}_4\text{I}_2\text{N}_{12}\text{O}_2$: $M_r = 984.42$, $0.20 \times 0.20 \times 0.12$ mm, triclinic, space group $P\bar{1}$, $a = 9.7340(19)$, $b = 10.415(2)$, $c = 10.673(2)$ Å, $\alpha = 106.70(3)^\circ$, $\beta = 91.28(3)^\circ$, $\gamma = 100.37(3)^\circ$, $V = 1016.3(4)$ Å³, $Z = 1$, $d_{\text{calcd.}} = 1.608$ Mg m⁻³, Mo- K_{α} radiation (graphite monochromated, $\lambda = 0.71073$ Å), $T = 100$ K, $\theta_{\text{range}} 2.00$ to 29.00° . Reflections measured 9567, independent 5317, $R_{\text{int}} = 0.0377$. Final R indices [$I > 2\sigma(I)$]: $R_1 = 0.0387$, $wR_2 = 0.0769$.

(4)I₂: Compound **4** (21.0 mg, 0.038 mmol) was dissolved in CH_2Cl_2 (5 mL). To this green solution was added I_2 (9.64 mg, 0.038 mmol). The solution turned purple immediately. Black crystals with a red metallic shine were obtained by layering the solution with Et_2O (5 mL). $\text{C}_{26}\text{H}_{40}\text{I}_2\text{N}_{12}\text{O}_2 \cdot \text{CH}_2\text{Cl}_2$ (891.42): calcd. C 36.38, H 4.75, N 18.86; found C 35.12, H 4.77, N 17.53. MS (HR-ESI⁺): m/z (%) = 679.24393 (100.0) $[\text{M} - \text{I}]^+$ (calcd. 679.24420), 552.33955 (41.9) $[\text{M} - \text{I}_2]^+$ (calcd. 552.33972). ¹H NMR (600.13 MHz, CD_3CN): $\delta = 3.75$ (s, 16 H, CH_2), 2.70 (s, 24 H, CH_3) ppm. ¹³C{¹H} NMR (150.90 MHz, CD_3CN), HSQC, HMBC: $\delta = 168.53$ (s, C=O), 168.05 (s, NCN), 152.22 (s, C_{ring}), 49.16 (t, CH_2) 32.98 (q, CH_3) ppm. IR (CsI): $\tilde{\nu} = 2963$ (w), 2925 (w), 2886 (w), 2806 (w), 1570 (s), 1560 (s), 1558 (s), 1491 (s), 1477 (s), 1419 (m), 1368 (m), 1348 (m), 1292 (m), 1262 (w), 1235 (w), 1205 (w), 1072 (s), 1018 (m), 965 (m), 875 (w), 798 (m), 765 (w), 733 (w), 680 (w), 646 (w), 609 (w), 581 (w), 537 (w), 502 (w), 419 (w) cm⁻¹. UV/Vis (CH_3CN): λ (ϵ , L mol⁻¹ cm⁻¹) = 575 (38556), ca. 522 (24269), 365 (6591), 285 (18604), 247 (29109) nm. Crystal data for **(4)I₂**, $\text{C}_{30}\text{H}_{46}\text{I}_2\text{N}_{14}\text{O}_2$: $M_r = 888.61$, $0.70 \times 0.50 \times 0.50$ mm, triclinic, space group $P\bar{1}$, $a = 9.776(2)$, $b = 10.030(2)$, $c = 10.209(2)$ Å, $\alpha = 90.82(3)^\circ$, $\beta = 109.23(3)^\circ$, $\gamma = 93.73(3)^\circ$, $V = 942.5(3)$ Å³, $Z = 1$, $d_{\text{calcd.}} = 1.566$ Mg m⁻³, Mo- K_{α} radiation (graphite monochromated, $\lambda = 0.71073$ Å), $T = 100$ K, $\theta_{\text{range}} 2.88$ to 35.00° . Reflections measured 14600, independent 8163, $R_{\text{int}} = 0.0335$. Final R indices [$I > 2\sigma(I)$]: $R_1 = 0.0370$, $wR_2 = 0.0925$.

[2(CuBr)₂]: Compound **2** (71.7 mg, 0.13 mmol) was dissolved in CH_3CN (8 mL). CuBr (38.7 mg, 0.27 mmol) was then added to the pale green solution. The reaction mixture was stirred at room temperature for 30 min. A pale green precipitate formed, which was

dissolved by briefly heating. Pale green crystals were isolated from the deep green reaction mixture. Yield: 70.2 mg, 0.09 mmol, 66%. $\text{C}_{25}\text{H}_{49}\text{Br}_2\text{Cu}_2\text{N}_{13}$ (818.64): calcd. C 36.68, H 6.03, N 22.24; found C 35.70, H 5.99, N 21.28. ¹H NMR (600.13 MHz, CD_3CN): $\delta = 5.87$ (s, 1 H, H_{Ar}), 2.78 (s, 48 H, CH_3) ppm. ¹³C{¹H} NMR (150.90 MHz, CD_3CN): $\delta = 163.26$ (s), 40.17 (q, CH_3) ppm. MS (FAB⁺): m/z (%) = 819.2 (26.00) $[\text{M}]^+$, 738.2 (68.00) $[\text{M} - \text{Br}]^+$, 676.2 (100.0) $[\text{M} - \text{CuBr} + \text{H}]^+$. IR (CsI): $\tilde{\nu} = 2995$ (w), 2933 (w), 2876 (w), 2792 (w), 1616 (m), 1541 (m), 1388 (m), 1151 (s), 1022 (vs), 896 (s), 719 (s) cm⁻¹. Crystal data for $\text{C}_{33}\text{H}_{61}\text{Br}_2\text{Cu}_2\text{N}_{17}$: $M_r = 982.89$, $0.40 \times 0.30 \times 0.25$ mm, monoclinic, space group $C2/c$, $a = 20.121(4)$, $b = 12.566(3)$, $c = 20.279(4)$ Å, $\beta = 116.55(3)^\circ$, $V = 4587(2)$ Å³, $Z = 4$, $d_{\text{calcd.}} = 1.423$ Mg m⁻³, Mo- K_{α} radiation (graphite monochromated, $\lambda = 0.71073$ Å), $T = 100$ K, $\theta_{\text{range}} 2.37$ to 30.00° . Reflections measured 25088, independent 6660, $R_{\text{int}} = 0.0774$. Final R indices [$I > 2\sigma(I)$]: $R_1 = 0.0673$, $wR_2 = 0.1614$ cm⁻¹.

[2(CuI)₂]: Compound **2** (30 mg, 0.056 mmol) was dissolved in CH_3CN (8 mL). CuI (21.5 mg, 0.113 mmol) was then added, and the reaction mixture stirred at room temperature for 30 min. A pale green precipitate formed, which was redissolved by briefly heating. Pale green crystals were isolated from the deep green reaction mixture. Yield: 48.0 mg, 0.052 mmol, 93%. $\text{C}_{25}\text{H}_{49}\text{Cu}_2\text{I}_2\text{N}_{13}$ (912.64): calcd. C 32.90, H 5.41, N 19.95; found C 32.74, H 5.41, N 19.30. ¹H NMR (199.92 MHz, CD_2Cl_2): $\delta = 5.75$ (s, 1 H, H_{Ar}), 2.80 (s, 48 H, CH_3) ppm. MS (FAB⁺): m/z (%) = 913.1 (6.896) $[\text{M}]^+$, 784.6 (26.21) $[\text{M} - \text{I}]^+$, 722.4 (25.51) $[\text{M} - \text{CuI}]^+$, 594.3 (13.79) $[\text{M} - \text{CuI} - \text{I}]^+$, 531.5 (100.0) $[\text{M}]^+$. IR (CsI): $\tilde{\nu} = 3001$ (w), 2936 (w), 2881 (w), 2794 (w), 1622 (m), 1558 (vs), 1521 (vs), 1448 (s), 1421 (vs), 1389 (vs), 1153 (vs), 1024 (vs), 898 (m), 707 (m) cm⁻¹. Crystal data for $\text{C}_{33}\text{H}_{61}\text{Cu}_2\text{I}_2\text{N}_{17}$: $M_r = 1076.89$, $0.30 \times 0.25 \times 0.25$ mm, monoclinic, space group $C2/c$, $a = 20.385(4)$, $b = 12.663(3)$, $c = 20.483(4)$ Å, $\beta = 117.02(3)^\circ$, $V = 4710(2)$ Å³, $Z = 4$, $d_{\text{calcd.}} = 1.519$ Mg m⁻³, Mo- K_{α} radiation (graphite monochromated, $\lambda = 0.71073$ Å), $T = 100$ K, $\theta_{\text{range}} 2.23$ to 30.09° . Reflections measured 40967, independent 6901, $R_{\text{int}} = 0.0638$. Final R indices [$I > 2\sigma(I)$]: $R_1 = 0.0388$, $wR_2 = 0.0975$.

[2(CuCN)₂]: Compound **2** (50 mg, 0.09 mmol) was dissolved in CH_3CN (8 mL). CuCN (16.8 mg, 0.19 mmol) was added, and the pale green reaction mixture was heated at reflux for 30 min. The reaction mixture was cooled to room temperature overnight; a yellow precipitate formed, which was dissolved by briefly heating. Yellow crystals suitable for an XRD analysis were isolated from the pale green reaction mixture. Yield: 47.3 mg, 0.07 mmol, 71%. $\text{C}_{27}\text{H}_{49}\text{Cu}_2\text{N}_{15}$ (710.87): calcd. C 45.62, H 6.95, N 29.56; found C 44.52, H 6.74, N 28.69. ¹H NMR (600.13 MHz, CD_2Cl_2): $\delta = 5.70$ (s, 1 H, H_{Ar}), 2.83 (s, 48 H, CH_3) ppm. ¹³C{¹H} NMR (150.90 MHz, CD_2Cl_2), HSQC, HMBC, DEPT: $\delta = 165.37$ (s, NCN), 162.74 (s, NCN), 147.83 (s, C_{Ar}), 129.99 (s, C_{Ar}), 115.81 (s, C_{Ar}), 40.28 (q, CH_3) ppm. MS (FAB⁺): m/z (%) = 709.9 (26.00) $[\text{M}]^+$, 685.6 (30.00) $[\text{M} - \text{CN} + \text{H}]^+$, 621.5 (35.00) $[\text{M} - \text{CuCN} + \text{H}]^+$, 594.5 $[\text{M} - \text{CuCN} - \text{CN}]^+$, 531.6 $[\text{M}]^+$. IR (CsI): $\tilde{\nu} = 3003$ (w), 2937 (w), 2882 (w), 2797 (w), 2103 (s), 1523 (vs), 1464 (s), 1424 (vs), 1392 (vs), 1246 (s), 1230 (s), 1156 (vs), 1027 (vs), 899 (s), 719 (s) cm⁻¹. UV/Vis (CH_3CN): λ (ϵ , L mol⁻¹ cm⁻¹) = 407 (17922), 331 (24609), 224 (56502) nm. Crystal data for $[\text{2}(\text{CuCN})_2] \cdot 4\text{CH}_3\text{CN}$, $\text{C}_{35}\text{H}_{61}\text{Cu}_2\text{N}_{19}$: $M_r = 875.13$, $0.30 \times 0.20 \times 0.20$ mm, monoclinic, space group $C2/c$, $a = 20.211(4)$, $b = 12.549(3)$, $c = 20.016(4)$ Å, $\beta = 115.68(3)^\circ$, $V = 4575(2)$ Å³, $Z = 4$, $d_{\text{calcd.}} = 1.271$ Mg m⁻³, Mo- K_{α} radiation (graphite monochromated, $\lambda = 0.71073$ Å), $T = 100$ K, $\theta_{\text{range}} 2.50$ to 27.55° . Reflections measured 36321, independent 5234, $R_{\text{int}} = 0.0494$. Final R indices [$I > 2\sigma(I)$]: $R_1 = 0.0452$, $wR_2 = 0.1084$.

FULL PAPER

[(2-I)(CuI)₂](I₃)₂]_n: I₂ (43.2 mg, 0.23 mmol) was added to a suspension of [2(CuI)₂] (74.9 mg, 0.08 mmol) in CH₃CN (8 mL). The colour of the reaction mixture turned immediately from dark green to black. The reaction mixture was stirred for 30 min, after which a black solid precipitated. The black solution was removed by syringe, and the precipitate was washed with CH₃CN. Yield (raw product): 112 mg, 76%, 0.06 mmol. C₂₅H₄₉Cu₂I₈N₁₃ (1674.07): calcd. C 17.94, H 2.95, N 10.88; found C 18.62, H 3.05, N 11.26. MS (ESI⁺): *m/z* (%) = 531.3 (4.85) [2]⁺, 265.8 (100.0) [2]²⁺. MS (ESI⁻): *m/z* (%) = 381.0 (40.68) [I₃]⁻, 127.2 (100.0) [I]⁻. IR (CsI): $\tilde{\nu}$ = 3013 (w), 2964 (w), 2829 (w), 2803 (w), 1617 (s), 1551 (s), 1510 (s), 1482 (vs), 1460 (vs), 1401 (vs), 1387 (vs), 1292 (vs), 1227 (w), 1173 (ss), 1064 (w), 1030 (m), 894 (w), 795 (w) cm⁻¹. UV/Vis (CH₃CN): λ (ϵ , L mol⁻¹ cm⁻¹) = 502 (4153), 364 (33517), 291 (46050), 245 (43998) nm.

[2(CuI)₂] + CH₃I: Methyl iodide (14.9 μ L, 34.0 mg, 0.24 mmol) was slowly added to a dark green suspension of [2(CuI)₂] (49.0 mg, 0.054 mmol) in acetone (3 mL) at room temperature. The reaction mixture was stirred further for 16 h at room temperature, but no reaction occurred. In another experiment methyl iodide (6.65 μ L, 15.2 mg, 0.11 mmol) was slowly added to a dark green suspension of [2(CuI)₂] (81.6 mg, 0.09 mmol) in acetonitrile (3 mL) at room temperature. The reaction mixture was heated to 48 °C for 8 h, but again no reaction occurred.

[3(CuI)(CuI₂)I]_n: CuI (13.58 mg, 0.07 mmol) was added to a solution of **3** (20 mg, 0.036 mmol) in CH₃CN (5 mL). The solution turned brown, and after 1 h, the solvent was removed. Black crystals could be obtained by slow evaporation of the solvent. Crystal data for [3(CuI)(CuI₂)I]_n, C₂₈H₅₁Cu₂I₄N₁₃O₂: *M_r* = 1236.50, 0.25 × 0.15 × 0.15 mm, triclinic, space group *P* $\bar{1}$, *a* = 13.057(3), *b* = 13.461(3), *c* = 13.699(3) Å, α = 75.89(3)°, β = 74.74(3)°, γ = 89.67(3)°, *V* = 2248.3(10) Å³, *Z* = 2, *d*_{calcd.} = 1.826 Mg m⁻³, Mo-*K α* radiation (graphite monochromated, λ = 0.71073 Å), *T* = 100 K, θ _{range} 2.18 to 27.57°. Reflections measured 18829, independent 10273, *R*_{int} = 0.0518. Final *R* indices [*I* > 2 σ (*I*)]: *R*₁ = 0.0603, *wR*₂ = 0.1510.

X-ray Crystallographic Study: Suitable crystals were taken directly out of the mother liquor, immersed in perfluorinated polyether oil and fixed on top of a glass capillary. Measurements were made on a Nonius-Kappa CCD diffractometer with a low-temperature unit using graphite-monochromated Mo-*K α* radiation. The temperature was set to 100 K. The data collected were processed by using the standard Nonius software.^[28] All calculations were performed by using the SHELXT-PLUS software package. Structures were solved by direct methods with the SHELXS-97 program and refined with the SHELXL-97 program.^[29,30] Graphical handling of the structural data during solution and refinement was performed with XPMA.^[31] Atomic coordinates and anisotropic thermal parameters of non-hydrogen atoms were refined by full-matrix least-squares calculations. Crystallographic data (excluding structure factors) for the structures reported in this paper have been deposited with the Cambridge Crystallographic Data Centre as supplementary publication nos. CCDC-843459 (**2**), -843455 (**3**), -843457 (**4**), -843458 [2-(β -hydroxyethylamino)-*p*-benzoquinone], 843461 ([2H₄]Cl₄), 843456 ([3H₄]Cl₄), 848206 ([2-(Br)H](Br₃)₂), 843460 ([2-I](I₃)₁), 843462 ([2-I]I₂), 843454 ([3]I₂), 886681 ([4]I₂), 843464 ([2(CuBr)₂]), 843463 ([2(CuI)₂]), 886682 [2(CuCN)₂], 886680 [3(CuI)(CuI₂)I]_n contain the supplementary crystallographic data for this paper. These data can be obtained free of charge from The Cambridge Crystallographic Data Centre via www.ccdc.cam.ac.uk/data_request/cif.

Details of the Quantum Chemical Calculations: All calculations were carried out with the aid of the GAUSSIAN 09 program.^[32]

All structures were optimized by using the structures derived experimentally in the crystalline phase as starting points if available, and vibrational frequencies were calculated. The calculations on the ΔG^0 values for the gas-phase redox reactions involving **1a**, **2**, **3** and **4** relied on the B3LYP functional^[33] and the 6-311G** basis set.^[34] The p*K_a* values in CH₃CN solutions were estimated according to the procedure of Maksić et al.^[24] First, the structures of the neutral and the protonated forms were optimized by using the B3LYP functional together with the 6-311G** basis set. Finally, the energies were retrieved from a B3LYP/6-311+G** calculation.^[33b,35] The calculations used the conductor-like polarizable continuum model to describe solvation by CH₃CN.

Supporting Information (see footnote on the first page of this article): Crystal structure of the benzoquinone derivative formed by elimination of two dimethylamino groups, UV/Vis spectrum of **2**, molecular structure of 2-(β -hydroxyethylamino)-*p*-benzoquinone, absorption and emission spectra of 2-(β -hydroxyethylamino)-*p*-benzoquinone, calculated structures and Gibbs free energy differences for two possible tautomers of [2H]⁺ and [3H]⁺ and fraction of the crystal structure of [2-I]I₂ are presented.

Acknowledgments

The authors gratefully acknowledge continuous financial support by the *Deutsche Forschungsgemeinschaft* (DFG).

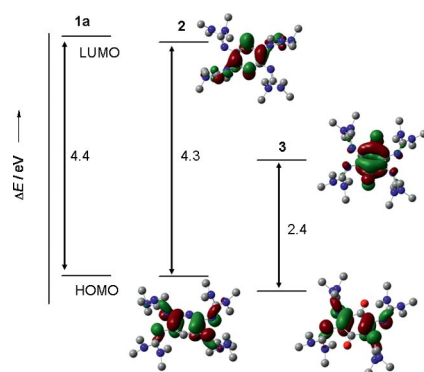
- [1] a) C. Wurster, *Ber. Dtsch. Chem. Ges.* **1879**, *12*, 522–528; b) C. Wurster, E. Schobig, *Ber. Dtsch. Chem. Ges.* **1879**, *12*, 1807.
- [2] a) K. Elbl, C. Krieger, H. A. Staab, *Angew. Chem.* **1986**, *98*, 1024–1026; *Angew. Chem. Int. Ed. Engl.* **1986**, *25*, 1023–1025; b) K. Elbl-Weiser, F. A. Neugebauer, H. A. Staab, *Tetrahedron Lett.* **1989**, *30*, 6161–6164; c) C. J. Adams, R. C. da Costa, C. Rosenildo, R. Edge, D. H. Evans, M. F. Matthew, *J. Org. Chem.* **2010**, *75*, 1168–1179.
- [3] a) T. Barth, C. Krieger, F. A. Neugebauer, H. A. Staab, *Angew. Chem.* **1991**, *103*, 1006–1008; *Angew. Chem. Int. Ed. Engl.* **1991**, *30*, 1028–1030; b) T. Barth, C. Krieger, H. A. Staab, F. A. Neugebauer, *J. Chem. Soc., Chem. Commun.* **1993**, 1129–1131; c) H. A. Staab, A. Kirsch, T. Barth, C. Krieger, F. A. Neugebauer, *Eur. J. Org. Chem.* **2000**, 1617–1622.
- [4] a) F. T. Edelmann, *Adv. Organomet. Chem.* **2008**, *57*, 183–352; b) F. T. Edelmann, *Coord. Chem. Rev.* **1994**, *137*, 403–481.
- [5] a) J. Barker, M. Kilner, *Coord. Chem. Rev.* **1994**, *133*, 219–300; b) P. J. Bailey, S. Price, *Coord. Chem. Rev.* **2001**, *214*, 91–141.
- [6] Herres-Pawlis, *Nachr. Chem.* **2009**, *57*, 20–23.
- [7] a) M. P. Coles, *Dalton Trans.* **2006**, 985–1001; b) M. P. Coles, *Chem. Commun.* **2009**, 3659–3676.
- [8] C. Jones, *Coord. Chem. Rev.* **2010**, *254*, 1273–1289.
- [9] H.-J. Himmel in *Modeling of Molecular Properties* (Ed.: P. Comba), Wiley-VCH **2011**.
- [10] a) J. Börner, U. Flörke, K. Huber, A. Döring, D. Kuckling, S. Herres-Pawlis, *Chem. Eur. J.* **2009**, *15*, 2362–2376; b) J. Börner, I. dos Santos Vieira, A. Pawlis, A. Doering, D. Kuckling, S. Herres-Pawlis, *Chem. Eur. J.* **2011**, *17*, 4507–4512; c) J. Börner, I. dos Santos Vieira, M. D. Jones, A. Döring, D. Kuckling, U. Flörke, S. Herres-Pawlis, *Eur. J. Inorg. Chem.* **2011**, 4441–4456; d) I. dos Santos Vieira, S. Herres-Pawlis, *Eur. J. Inorg. Chem.* **2012**, 765–774; e) I. dos Santos Vieira, S. Herres-Pawlis, *Z. Naturforsch. B* **2012**, *67*, 320–330.
- [11] a) M. Schatz, V. Raab, S. P. Foxon, G. Brehm, S. Schneider, M. Reiher, M. C. Holthausen, J. Sundermeyer, S. Schindler, *Angew. Chem.* **2004**, *116*, 4460–4464; *Angew. Chem. Int. Ed.* **2004**, *43*, 4360–4363; b) Ch. Würtele, E. V. Gaoutchenova, K. Harms, M. C. Holthausen, J. Sundermeyer, S. Schindler, *Angew. Chem.* **2006**, *118*, 3951–3954; *Angew. Chem. Int. Ed.* **2006**, *45*, 3867–3869; c) D. Maiti, D.-H. Lee, K. Gaoutchenova, C. Würtele,

- M. C. Holthausen, A. A. Narducci Sarjeant, J. Sundermeyer, S. Schindler, K. D. Karlin, *Angew. Chem.* **2007**, *120*, 88–91; *Angew. Chem. Int. Ed.* **2007**, *47*, 82–85; d) D. Maiti, D.-H. Lee, A. A. Narducci Sarjeant, M. Y. M. Pau, E. I. Solomon, K. Goutchenova, J. Sundermeyer, K. D. Karlin, *J. Am. Chem. Soc.* **2008**, *130*, 6700–6701; e) J. S. Woertink, L. Tian, D. Maiti, H. R. Lucas, R. A. Himes, K. D. Karlin, F. Neese, C. Würtele, M. C. Holthausen, E. Bill, J. Sundermeyer, S. Schindler, E. I. Solomon, *Inorg. Chem.* **2010**, *49*, 9450–9459.
- [12] A. Peters, E. Kaifer, H.-J. Himmel, *Eur. J. Org. Chem.* **2008**, 5907–5914.
- [13] a) A. Peters, C. Trumm, M. Reinmuth, D. Emeljanenko, E. Kaifer, H.-J. Himmel, *Eur. J. Inorg. Chem.* **2009**, 3791–3800; b) D. Emeljanenko, A. Peters, N. Wagner, J. Beck, E. Kaifer, H.-J. Himmel, *Eur. J. Inorg. Chem.* **2010**, 1839–1846; c) C. Trumm, E. Kaifer, O. Hübner, H.-J. Himmel, *Eur. J. Inorg. Chem.* **2010**, 3102–3108.
- [14] a) M. Reinmuth, U. Wild, E. Kaifer, M. Enders, H. Wadepohl, H.-J. Himmel, *Eur. J. Inorg. Chem.* **2009**, 4795–4808; b) P. Roquette, C. König, O. Hübner, A. Wagner, E. Kaifer, M. Enders, H.-J. Himmel, *Eur. J. Inorg. Chem.* **2010**, 4770–4782; c) D. Emeljanenko, E. Kaifer, H. Wadepohl, H.-J. Himmel, *Eur. J. Inorg. Chem.* **2012**, 695–704; d) C. Trumm, S. Stang, B. Eberle, E. Kaifer, N. Wagner, J. Beck, T. Bredow, N. Meyerbröker, M. Zharnikov, O. Hübner, H.-J. Himmel, *Eur. J. Inorg. Chem.* **2012**, 3156–3167.
- [15] A. Peters, H. Herrmann, M. Magg, E. Kaifer, H.-J. Himmel, *Eur. J. Inorg. Chem.* **2012**, 1620–1631.
- [16] Y. Wang, Z. Hu, X. Meng, J. Jing, Y. Song, C. Zhang, Y. Huang, *Molecules* **2009**, *14*, 1652–1659.
- [17] K. Wallenfels, W. Draber, *Tetrahedron Lett.* **1959**, *10*, 24–25.
- [18] E. Winkelmann, *Tetrahedron* **1969**, *25*, 2427–2454.
- [19] H. Bock, K. Ruppert, C. Näther, Z. Havlas, *Angew. Chem.* **1991**, *103*, 1194–1197; *Angew. Chem. Int. Ed. Engl.* **1991**, *30*, 714–717.
- [20] a) A. Bolovinos, P. Tsekeris, J. Philis, E. Pantos, G. Andritsopoulos, *J. Mol. Spectrosc.* **1984**, *103*, 240–246; b) I. C. Walker, M. H. Palmer, A. Hopkirk, *Chem. Phys.* **1989**, *141*, 365–378.
- [21] K.-H. König, *Chem. Ber.* **1959**, *92*, 257–267.
- [22] G. Löber, *Z. Phys. Chem. (Leipzig)* **1966**, *231*, 123–134.
- [23] K. Wallenfels, W. Draber, *Angew. Chem.* **1958**, *70*, 313.
- [24] B. Kovačević, Z. B. Maksić, *Org. Lett.* **2001**, *3*, 1523–1526.
- [25] D. Emeljanenko, A. Peters, V. Vitske, E. Kaifer, H.-J. Himmel, *Eur. J. Inorg. Chem.* **2010**, 4783–4789.
- [26] H. Isci, W. R. Mason, *Inorg. Chem.* **1985**, *24*, 271–274.
- [27] For a more detailed discussion about metal–guanidine bonding, see: P. Roquette, A. Maronna, A. Peters, E. Kaifer, H.-J. Himmel, C. Hauf, V. Herz, E.-W. Scheidt, W. Scherer, *Chem. Eur. J.* **2010**, *16*, 1336–1350.
- [28] DENZO-SMN, Data processing software, Nonius **1998**; <http://www.noniuss.com>.
- [29] G. M. Sheldrick, *SHELXS-97* and *SHELXL-97*, Program for Crystal Structure Solution, University of Göttingen, **1997**; <http://shelx.uni-ac.gwdg.de/SHELX/index.html>.
- [30] *International Tables for X-ray Crystallography*, Vol. 4, Kynoch Press, Birmingham, U. K., **1974**.
- [31] L. Zsolnai, G. Huttner, *XPMA*, University of Heidelberg, **1994**; <http://www.uni-heidelberg.de/institute/fak12/AC/huttner/software/software.html>.
- [32] M. J. Frisch, G. W. Trucks, H. B. Schlegel, G. E. Scuseria, M. A. Robb, J. R. Cheeseman, G. Scalmani, V. Barone, B. Mennucci, G. A. Petersson, H. Nakatsuji, M. Caricato, X. Li, H. P. Hratchian, A. F. Izmaylov, J. Bloino, G. Zheng, J. L. Sonnenberg, M. Hada, M. Ehara, K. Toyota, R. Fukuda, J. Hasegawa, M. Ishida, T. Nakajima, Y. Honda, O. Kitao, H. Nakai, T. Vreven, J. A. Montgomery Jr., J. E. Peralta, F. Ogliaro, M. Bearpark, J. J. Heyd, E. Brothers, K. N. Kudin, V. N. Staroverov, R. Kobayashi, J. Normand, K. Raghavachari, A. Rendell, J. C. Burant, S. S. Iyengar, J. Tomasi, M. Cossi, N. Rega, J. M. Millam, M. Klene, J. E. Knox, J. B. Cross, V. Bakken, C. Adamo, J. Jaramillo, R. Gomperts, R. E. Stratmann, O. Yazyev, A. J. Austin, R. Cammi, C. Pomelli, J. W. Ochterski, R. L. Martin, K. Morokuma, V. G. Zakrzewski, G. A. Voth, P. Salvador, J. J. Dannenberg, S. Dapprich, A. D. Daniels, O. Farkas, J. B. Foresman, J. V. Ortiz, J. Cioslowski, D. J. Fox, *Gaussian 09*, Revision A.02, Gaussian Inc., Wallingford CT, **2009**.
- [33] a) P. J. Stephens, F. J. Devlin, C. F. Chabalowski, M. J. Frisch, *J. Chem. Phys.* **1994**, *98*, 11623–11627; b) A. D. Becke, *J. Chem. Phys.* **1993**, *98*, 5648–5652; c) C. Lee, W. Yang, R. G. Parr, *Phys. Rev. B* **1988**, *37*, 785–789.
- [34] a) R. Krishnan, J. S. Binkley, R. Seeger, J. A. Pople, *J. Chem. Phys.* **1980**, *72*, 650–654; b) A. D. McLean, G. S. Chandler, *J. Chem. Phys.* **1980**, *72*, 5639–5648.
- [35] a) K. Raghavachari, J. S. Binkley, R. Seeger, J. A. Pople, *J. Chem. Phys.* **1980**, *72*, 650–654; b) M. J. Frisch, J. A. Pople, J. S. Binkley, *J. Chem. Phys.* **1984**, *80*, 3265–3269.

Received: June 21, 2012

Published Online: ■

Three new members of the family of redox-active guanidine ligands are presented, and their redox potential as well as aspects of their coordination chemistry studied.



S. Stang, A. Lebkücher, P. Walter,
E. Kaifer, H.-J. Himmel* 1–14

Redox-Active Guanidine Ligands with
Pyridine and *p*-Benzoquinone Backbones



Keywords: Guanidine / Redox chemistry /
Coordination compounds / Copper / Den-
sity functional calculations